

---

# THE COMPUTATIONAL PATIENT HAS DIABETES AND A COVID

---

A PREPRINT

**Pietro Barbiero\***

Department of Computer Science and Technology, University of Cambridge, Cambridge, UK  
 pietro.barbiero@tutanota.com

**Pietro Lió**

Department of Computer Science and Technology, University of Cambridge, Cambridge, UK  
 pl219@cam.ac.uk

November 10, 2021

## ABSTRACT

Medicine is moving from reacting to a disease to prepare personalised and precision paths to well being. The complex and multi level pathophysiological patterns of most diseases require a systemic medicine approach and are challenging current medical therapies. Computational medicine is a vibrant interdisciplinary field that could help moving from an organ-centered to a process-oriented or systemic medicine data analysis. The resulting Computational patient may require an international interdisciplinary effort, probably of larger scientific and technological interdisciplinarity than the human genome sequencing. When deployed, it will have a profound impact on how healthcare is delivered to patients. Here we present a Computational patient model that integrates, refine and extend recent specific mechanistic or phenomenological models of cardiovascular, RAS and diabetic processes. Our aim is twofold: analyse the modularity and composability of the models-building blocks of the Computational patient and to study the dynamical properties of well-being and disease states in a broader functional context. We present results from a number of experiments among which we characterise the dynamical impact of covid-19 and T2D diabetes on cardiovascular and inflammation conditions. We tested these experiments under exercise and meals and drug regimen. We report results showing the striking importance of transient dynamical responses to acute state conditions and we provide guidelines for system design principle of the inter-relationship between modules and components for systemic medicine. Finally this initial Computational Patient can be used as a toolbox for further modifications and extensions.

**Keywords** Computational Patient · Computational Medicine · Systems medicine · Covid · T2D Diabete · Cardiovascular model · Blood Pressure model

## 1 Introduction

Computational medicine is increasingly effective to understand and predict complex physiological and pathological conditions in scenarios of single organ disease to comorbidities. Important aspects of computational medicine are mechanistic and phenomenological models. When we formulate hypotheses on the mechanisms (usually involving molecules) underlying the behaviour of the various endpoints of a process, we could build a mechanistic model; when we formulate hypotheses based on the empirical observations of a phenomenon, we could build a phenomenological model. Most models are actually a combination of the two and there are certainly overlaps between phenomenological modeling, statistical and machine learning. Mechanistic and phenomenological modeling aim at reproducing the main features of a real system with the minimum number of parameters and still providing explainability, interpretability

---

\*Use footnote for providing further information about author (webpage, alternative address)—*not* for acknowledging funding agencies.

and often causality. The objective is to gain a better understanding of how each of the different components of a biomedical system contributes to the overall process, its emerging properties and the causality relation of the occurred events. A mechanistic and phenomenological model could be formulated using ordinary or partial differential equations [1], stochastic processes [2], logic [3] or in terms of a tailor-made syntax which could facilitate formal analysis and verification [4, 5]. The dedicated modeler may introduce a series of models of a process at different scales, from the molecular level to the whole body level, or describing processes occurring in different organs under the same disease conditions. Although there is growing awareness of long range communications in the body - for instance the communicome [6] or the gut-brain axis [7], the integration of various models in order to capture the behavior at systems medicine level has not been pursued so much. Examples of such multi level communication are given by the extensive network of comorbidities. Comorbidity is the term used to address diseases, often chronic ones, co-occurring in the same individual. An importance challenge is the homogenisation of models across multiple spatial and time scales, which requires cell-level models to be systematically scaled up to the tissue/organ level, and related asymptotic techniques for the analysis of multiple timescale problems, such as those arising in processes communications. The cardiovascular system is usually described using a cardio-centric view. The heart is considered as the only pump in the system. Other pumps are actually the skeletal muscle which returns blood from the periphery to the central circulation. Another pump is embedded in the elastic arteries that use elastic properties to propel the blood forward. This system is subtly coupled with the cardiovascular-associated nervous system and the blood pressure control which include the regulated inputs from many other organs, most notably lungs, kidney and pancreas [8]. Therefore, the concept of cardiovascular disease could be reformulated as a more complexly connected system and disease landscape, perhaps inclusive of comorbidities, which could allow a better patient stratification and prognosis and consequently better drug discovery.

In particular infectious diseases are good examples of the need of inter organ and inter process modeling approaches as a pathogen's fitness may require colonising different body's environments. A current example is given by the COVID-19 pandemia. Diabetes is a frequent comorbidity; the Coronado study has shown that 29% of the people with T2D infected with Covid-19 were intubated and 10.6% die in one week [9]. The mortality statistics shows that fighting the COVID-19 pandemia requires a focus on comorbidities. Many of the older patients who become severely ill have evidence of underlying illness such as cardiovascular disease, kidney disease, T2D or tumours [10]. They make the largest percentage of patient who cannot breathe on their own because of severe pneumonia and acute respiratory distress syndrome and require intubation: about a quarter of intubated coronavirus patients dies within the first few weeks of treatment [11].

## 2 Objectives

The aim of this work is twofold. First, in Sec. 3 we propose a modular approach for the design of personalised computational physiology systems. The complexity underlying multifactorial diseases requires the introduction of multi-scale, extensible and adaptable models where modular principles are used to break organism complexity and composable criteria to select, link and combine different components in a hierarchical fashion. In order to show the advantages of such modeling approach, in Sec. 6 we illustrate a concrete example where personalised comorbid conditions' dynamics can be modeled and analysed using our framework. We focus on developing an integrated computational system modeling ripple effects of comorbidities on blood pressure regulation. To this end, in Sec. 4 we revised the physiological background required to understand the main underlying biological processes involved in this mechanism. Building upon previous studies, we devise a customisable Computational patient in the form of a computational tool composed of extended versions of three publicly available mathematical models describing the circulatory system [12], type-2 diabetes [13], and renin-angiotensin system (RAS) [14], one of the main pathways regulating inflammatory response and blood pressure. Respiratory failure is a key feature of severe Covid-19 and a critical driver of mortality; 10.6% of all diabetic patients hospitalised die within one week. Hence, in Sec. 5 we propose a set of equations modeling the impact of type 2 diabetes on blood vessels' stiffness and the influence of additional external factors which can be personalised according to patient's characteristics and lifestyle habits. We introduce a variety of such elements describing the repercussions on blood pressures caused by ageing, type-2 diabetes, viral infections like COVID19, ACE inhibitor treatments, meals, and physical exercise.

## 3 Computational tool

### 3.1 From integration to modularity and composability

In the last decades, the interest and the scientific effort in developing integrated quantitative and descriptive computational systems modeling physiological dynamics has rapidly grown. By 1997 the Physiome Project [15] and the EuroPhysiome Initiative [16] have actively devised and organised rich collections of mathematical models describing

the functional behavior of components of living organisms, such as organs, cell systems, biochemical reactions, or endocrine systems. Such modular approach has been primarily used to reduce complexity by deconvolving the human physiome into elementary subunits. Indeed, each computational module can be seen as a standalone biological entity describing one of the structures, processes, or pathways of the whole organism. Yet, modeling physiological interactions, multi-scale signalling, and comorbidities requires the combination of multiple components to build more sophisticated computational systems. Several approaches have been proposed where different mathematical models have been integrated into a single system in order to describe synergistic effects and emerging phenomena [12]. Despite being widely used and accepted, such system design paradigm often requires an overwhelming amount of work in merging multiple systems together, and in tuning and validating the integrated model. Besides, technological advances in computer science in the last twenty years have dramatically changed coding languages and paradigms. Hence, different research groups have developed their computational systems on many different coding platforms, frameworks, and libraries, including general-purpose languages like MatLab, Java, Python, C, but also special-purpose ones like JSim. The variety of implementation platforms combined with the mathematical effort required to merge many different systems is in conflict with the urgent need of user-friendly, extensible, and adaptable system design paradigms where components can be selected and assembled in various combinations to satisfy specific requirements. Personalised medicine requires the introduction of novel system design paradigms where modules break organism complexity and composable criteria are used to select and combine different components. Instead of merging, tuning, and validating the whole integrated system, each module could be tuned and validated independently. Composable criteria may allow researchers to primarily focus on multi-scale signalling between modules. Tuning and validation may apply just on inter-module signals which will make the overall system independent on module-specific implementation characteristics.

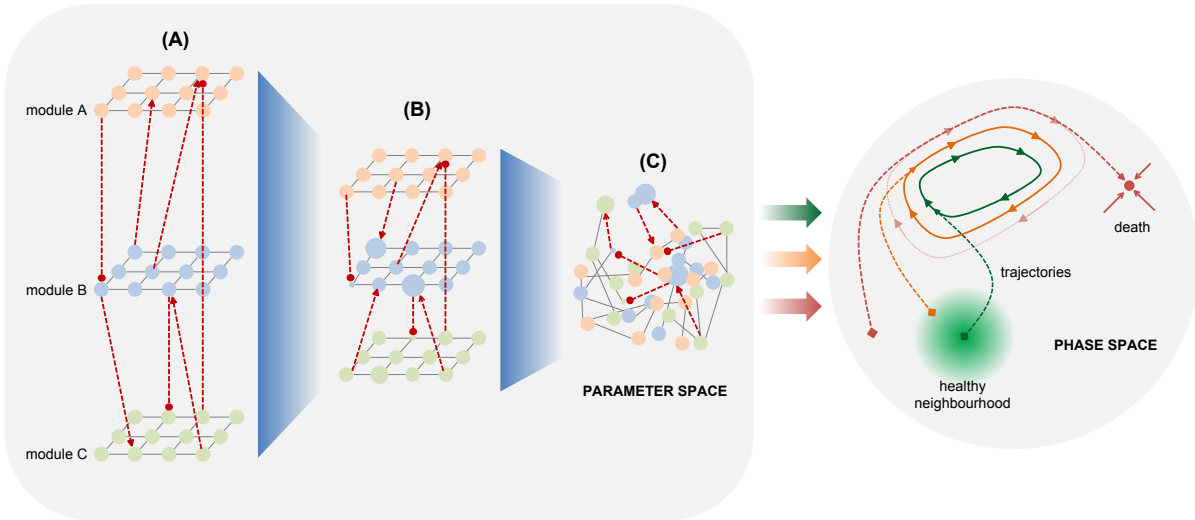


Figure 1: In modular systems several modules can be used independently to model physiological processes, disregarding their mutual relationships (A). The selection and combination of different components in a hierarchical fashion by means of composable criteria allows a better exploration of the parameter space (B). The actual interpenetration of multiple systems can be achieved by modeling the dynamics of their mutual relationships providing further information on the underlying phenomena (C). Such deeper exploration of the parameter space enhances the evaluation of initial conditions and trajectories in the phase space (right).

Figure design inspired by [17].

### 3.2 Module design and personalisation

In order to move towards this modern system design, each module can be seen as a black box processing signals coming from other modules and combining them with external subject-specific parameters in order to provide a set of responses (see Fig. 2). Subject-specific parameters may be derived from on-line clinically relevant measures, such as heart pressure or insulin levels, or from patient's medical records, such as morbidities, treatments, or clinical examinations. Such elements can be used to personalise the module taking into account unique subject characteristics. Incoming

signals from other components may impact some of the variables and parameters of the module, but cannot change its architecture. Finally, the outputs provided by each module can be simultaneously used as inputs for other components or tracked as clinically relevant latent variables.

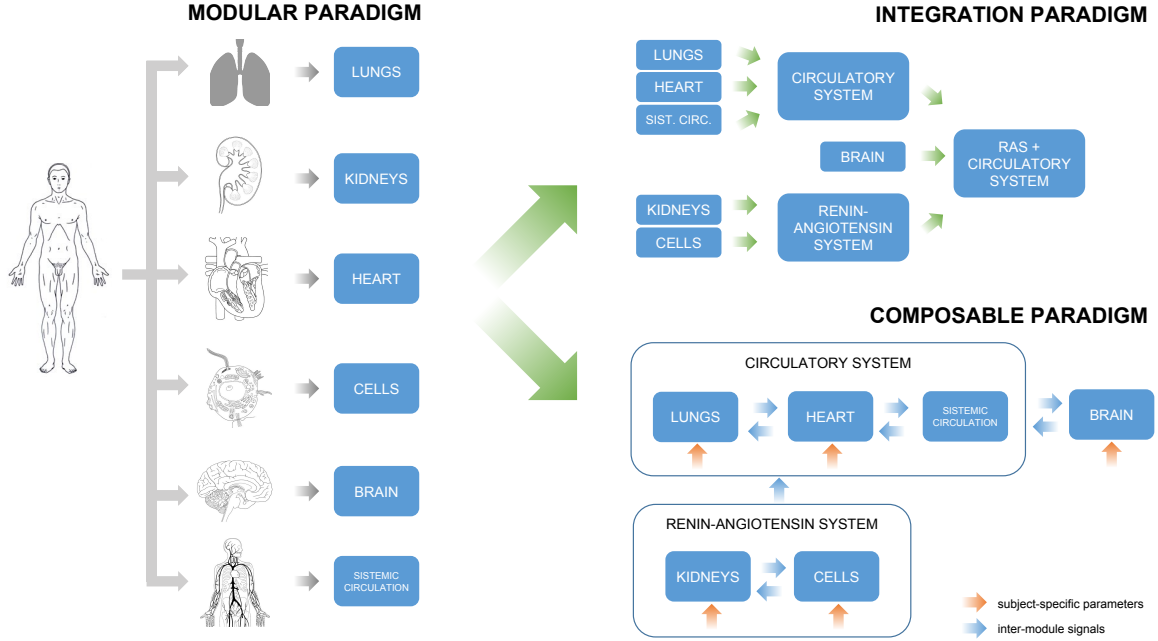


Figure 2: Modular paradigms are used to break organism complexity into simpler components which can be analysed and modeled independently (**left**). Modules’ integration requires an overwhelming amount of work in merging one after the other multiple systems together, and in tuning and validating the final model (**top right**). Composable criteria favor a dynamic and adaptable selection of different components allowing researchers to primarily focus on modeling the relationships between modules (**bottom right**).

Illustrations adapted from *The Sourcebook of medical illustration* [18].

### 3.3 Usage guidelines

The computational system has been designed in order to allow for three levels of user interaction. Computational scientists and coders may take advantage of publicly available code by improving or forking the GitHub repository [19]. The repository structure has a modular design so that new packages can be included independently. Each new package should correspond to a new mathematical model. Multiple packages can be combined together in order to generate more complex computational systems. Medical practitioners and biologists with some Python experience may just download the repository, reproduce the simulations on their computers, or modify some parameters. In order to make the computational tool available for clinicians and practitioners without coding skills, the whole computational system has been incorporated into a website with a graphical user interface. Users may profit from this user-friendly interaction as the system can be customised in many different ways creating multiple scenarios by modifying several parameters, including patient-specific characteristics and constants related to models’ interactions.

### 3.4 Numerical methods

All the necessary code for the experiments has been implemented in Python 3, relying upon open-source libraries. The mathematical equations described in Sec. 5 form a set of ODE systems and algebraic equations that have been sequentially solved using the LSODA integration method [20, 21] provided by the function `solve_ivp` included into the `scipy` Python package [22]. All the experiments have been run on the same machine: Intel® Core™ i7-8750H 6-Core Processor at 2.20 GHz equipped with 8 GiB RAM.

## 4 Physiological background

### 4.1 The link between hypertension, oxygenation and blood pressure variability

Exposure to chronic hypoxia causes pulmonary hypertension and pulmonary vascular remodelling [23]. Covid results in decreased oxygen that can result in impaired functioning of the heart and brain and cause difficulty with breathing (a PaO<sub>2</sub> reading below 80 mm Hg or a pulse ox (SpO<sub>2</sub>) below 95 percent is considered low). When the left side of the heart cannot pump blood out to the body normally, blood backs up in the lungs and increases blood pressure there. The covid19 virus can activate the blood clotting pathway. Studies have reported that 30% COVID-19 patients showed signs of blood clots in their lungs which means that a blood clot that has traveled to the lung. One of the recommendations is to give a low dose of heparin, which prevents clot formation or tissue plasminogen activator (tPA), which helps to dissolve blood clots. High blood pressure can damage the arteries by making them less elastic, which decreases the flow of blood and oxygen and leads to heart disease. The relationship between blood pressure and stroke recurrence is controversial. Recent researches stress that both high mean value of blood pressure and blood pressure variability (particularly long term) are important. Although some variation in blood pressure throughout the day is normal, higher variation in blood pressure is associated with a higher risk of cardiovascular disease and all-cause mortality [24, 25]. In young people there is an increased blood supply response to hypoxia which could vanish in elderly with high blood pressure. This compromised response may be caused by the high blood pressure-induced impairment in the function of the blood vessels [26].

#### 4.1.1 Arterial stiffness

Blood pressure variability and arterial stiffness independently predict cardiovascular risk [27, 28, 29, 30, 31]. Ageing increases arterial stiffness and that increased arterial stiffness gives rise to increased blood pressure variability [32]. Arterial stiffness is a broad term used to describe loss of arterial compliance and changes in vessel wall properties. Although arterial stiffness can be assessed using a variety of techniques, carotid–femoral pulse wave velocity is the preferred measure. It has been shown that increased arterial stiffness is an early risk marker for developing type 2 diabetes [33], and a causal association between T2D and increased arterial stiffness has been proved on a large cohort of patients [34, 35]: 1 standard deviation increase in T2D is associated with 6% higher risk in increased arterial stiffness; see also [36]. Arterial stiffness is also related to Inflammageing which is a chronic low-grade inflammation that develops with advanced age. It is believed to accelerate the process of biological ageing and to worsen many age-related diseases [37, 38]. In particular inflammatory cytokines (which may be activated by angiotensinII) result in increased arterial stiffness; on the contrary reductions in inflammation (for example due to anti-inflammatory cytokines), exercise reduce arterial stiffness [39, 40].

### 4.2 The renin-angiotensin system and SARS-CoV-2

The renin-angiotensin system (RAS) is a hormone system regulating vasoconstriction and inflammatory response [41]. The key regulator of the RAS is the peptide hormone Angiotensin II (ANG-II) generated by the angiotensin-converting enzyme (ACE) which cleaves the decapeptide Angiotensin I (ANG-I), or proangiotensin. ANG-II exerts its biological functions through two G-protein-coupled receptors, the ANG-II receptor type 1 receptor (AT1R) and ANG-II receptor type 2 receptor (AT2R), and the heptapeptide Angiotensin (1-7) (ANG-(1-7)) which binds and activates the G-protein-coupled Mas receptor (MAS). ANG-(1-7) can be generated both by the angiotensin-converting enzyme 2 (ACE2) from ANG-II, or by the neutral endopeptidase enzyme (NEP) from ANG-I. The three G-protein-coupled receptors (AT1R, AT2R, and MAS) are the main factors regulating blood pressure and systemic vascular resistance [42][43]. On one side, AT1R stimulates vasoconstriction, hypertension, and inflammatory response. The effect of AT1R is counterbalanced by AT2R and MAS, promoting vasodilation, hypotension, and vasoprotection. External factors impacting the RAS include: glucose concentration, ACE inhibitor treatments, and viral infections binding to ACE2, such as SARS-CoV-2. The glucose concentration has a direct impact both on AT1R and ACE activity. Hence, a high glucose concentration may determine chronic hypertensive conditions. Therefore, hypertensive treatments usually include ACE inhibitor drugs which are used to compensate the overproduction of ANG-II and AT1R [44]. Viral infections such as COVID19 may also have a negative impact on RAS [45], as the virus binds to ACE2 in order to gain entry into the host cell, impairing the activity of ACE2 in generating ANG-(1-7) by hydrolyzing ANG-II.

## 5 Mathematical model of diabetic Computational patients

In this section we describe the set of mathematical models used to model the diabetic Computational patient, i.e. RAS 5.1, diabetic 5.2, circulatory 5.3, and stiffness 5.4 models. Fig. 3 shows a schematic representation of the computational system. The Computational patient can be customised in two different ways. First, the system has been designed in

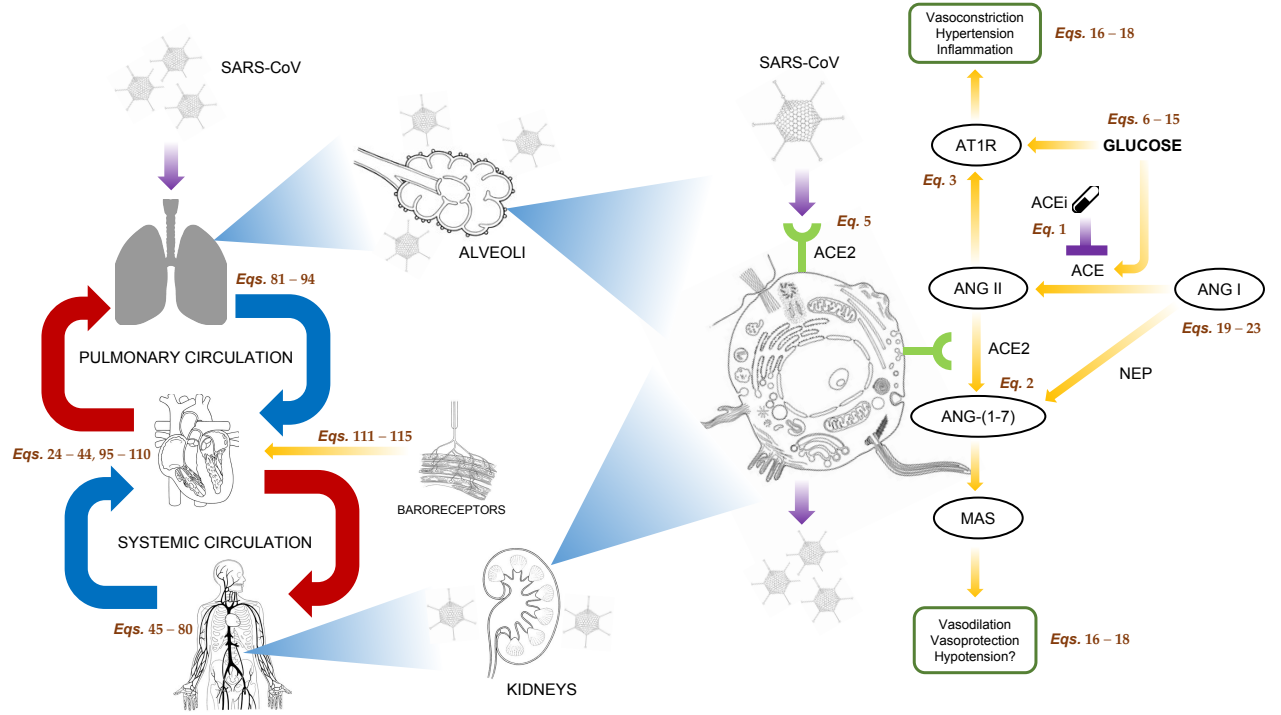


Figure 3: Schematic representation of the circulatory system composed of heart, pulmonary circulation, systemic circulation, and baroreceptors (**left**). External factors affecting the renin-angiotensin system (ACEi and SARS-CoV-2) are shown in **violet** (**right**).

Illustrations adapted from *The Sourcebook of medical illustration* [18].

order to be personalised using patient-specific values for some parameters such as age, glucose levels, arterial blood pressure, presence of comorbidities or treatments (see Table 1). Should the physiological analysis require the inclusion of additional conditions, new modules can be included and composed according to patient's needs.

Table 1: Computational patients' customisable parameters.

Class	Parameter	Description	Values	Units
Clinical record	$A$	Age	20 – 70	years
	$Glucose$	Blood glucose levels	100 – 200	$ml/dl$
	$ABP$	Arterial blood pressure (from clinical records, e.g. [12])	80 – 120	$mmHg$
Comorbidities	$infection$	Presence/absence of SARS-CoV-2 infection	{True, False}	-
	$renal$	Normal/impaired renal function	{True, False}	-
Treatments	$drug$	Presence/absence of ACEi treatments	{True, False}	-
	$d$	ACEi dosage (Benazepril)	0 – 5	$mg$
	$n_d$	Number of daily drug administrations	{0, 1}	-
Lifestyle	$t_w$	Daily workout starting time	6 p.m.	-
	$z_w$	Daily workout intensity (burned calories)	200	$kcal$
	$t_m$	Daily meals' starting time	{8 a.m. , 12 p.m. , 8 p.m.}	-
	$g_m$	Daily meals' glycemic load	{4, 42, 42}	-
	$s_m$	Daily meals' carbohydrate serving	{50, 100, 100}	$g$



## 5.1 Renin-angiotensin system and blood pressure regulation

The biochemical reaction network used to model the renin-angiotensin system is shown in Fig. 3. External factors include hypertension treatments and viral infections binding to ACE2, such as SARS-CoV-2. Hypertension drugs usually target ACE inhibiting ANG II production. ANG II promotes vasoconstriction, hypertension, inflammation, and fibrosis by activating AT1R. Therefore, reducing ANG II production with ACE inhibitors increases vasodilation and vasoprotection effects stimulated by AT2R and ANG-(1-7). On the other hand, SARS-CoV-2 infections reduce ANG-(1-7) and ANG-(1-9) production rate, by binding to ACE2 in order to gain entry into the host cell. Hence, vasoprotection effects promoted by ANG-(1-7) decline, possibly leading to hypertension and inflammatory response.

### 5.1.1 Pharmacokinetic model

Pharmacokinetic (PK) models are used to describe drugs absorption and excretion dynamics. Equation 1 describes the analytical solution of a single-compartment pharmacokinetic model with first-order absorption and first-order elimination rates after oral administration [46]. The equation has been used to model ACE inhibitors' dynamics and their effects on the RAS. A uniform dose size  $d$  at constant time intervals  $\tau$  has been assumed [47]:

$$[Drug]_n(t') = d \frac{k_a F}{(k_a - k_e) V} \left( \frac{1 - \exp(-nk_e \tau)}{1 - k_e \tau} \exp - k_e t' - \frac{1 - \exp(-nk_a \tau)}{1 - k_a \tau} \exp - k_a t' \right) \quad (1)$$

where  $[Drug]_n(t')$  is the drug concentration after the  $n$ -th dose,  $t' = t(n-1)\tau$  is the time after the  $n$ -th dose,  $k_a$  and  $k_e$  are the absorption and elimination rates respectively,  $F$  is the absorbed fraction of the drug, and  $V$  the volume of distribution.

Pharmacokinetic parameters have been reported in table 3.

### 5.1.2 Pharmacodynamic model

Pharmacodynamic models are used to illustrate the effects of drug treatments on the body. The pharmacodynamic model used to describe local RAS dynamics has been derived from [48, 14] (see Eqs. 15-19). The original model has been extended with four additional equations (Eqs. 2-5). The variation of  $[ANG17]$ ,  $[AT1R]$  and  $[AT2R]$  have been included as their dynamics can be useful in understanding how RAS regulates blood pressure [49]. The concentration of ANG-(1-7) depends on the activity of two enzymes, NEP and ACE2, cleaving ANG-I and ANG-II respectively.  $[AT1R]$  and  $[AT2R]$  rather depend on  $[ANGII]$  and on glucose concentration  $G$ .

$$\frac{d[ANG17]}{dt} = \overbrace{k_{NEP}[ANGI]}^{\text{NEP-catalyzed conversion of ANG I}} + \overbrace{k_{ACE2}[ANGII]}^{\text{ACE2-catalyzed conversion of ANG II}} - \overbrace{\frac{\ln 2}{h_{ANG17}}[ANG17]}^{\text{degradation}} \quad (2)$$

$$\frac{d[AT1R]}{dt} = \overbrace{\left(a_{AT1R}G + b_{AT1R}\right)[ANGII]}^{\text{ANG-II bounds}} - \overbrace{\frac{\ln 2}{h_{AT1R}}[AT1R]}^{\text{degradation}} \quad (3)$$

$$\frac{d[AT2R]}{dt} = \overbrace{k_{AT2R}[ANGII]}^{\text{ANG-II bounds}} - \overbrace{\frac{\ln 2}{h_{AT2R}}[AT2R]}^{\text{degradation}} \quad (4)$$

The dynamics of ACE2 activity ( $k_{ACE2}$ ) has been introduced as an indicator of SARS-CoV-2 infectivity [45]:

$$\frac{dk_{ACE2}}{dt} = \begin{cases} s_V[ANGII] - e_{AI}k_{ACE2} & \text{during SARS-CoV-2 infection} \\ 0 & \text{otherwise} \end{cases} \quad (5)$$

where  $s_V$  represents the severity of the viral infection and  $e_{AI}$  the efficiency of anti-inflammatory pathways. A higher concentration of  $[ANGII]$  may also induce cells to produce more ACE2, thus increasing its activity [45] and enhancing viral entry. Hence ACE-inhibitor treatments may have a protective role as they reduce ACE activity lowering ANG-II levels (see Fig. 3).

Pharmacodynamic parameters and initial conditions have been reported in table 4.

## 5.2 Adding comorbidities: Type 2 Diabetes

Type 2 diabetes is a metabolic progressive disease over time whose progression and severity is caused by increasing failure of insulin-production due to beta cell death.

There are complex multifactorial links between diabetes and cardiovascular disease [50, 51, 52, 53]. The main pathophysiology cornerstone is a state of chronic, low-level inflammation. This immune activation may facilitate both the insurgence and progression of insulin resistance in diabetic and pre-diabetic states and increases their cardiovascular risk. An extension of a model from Topp and collaborators (Eqs. 6-9) combines insuline resistance, functional  $\beta$ -cell mass dynamics with glucose dynamics and insulin dynamics [13]. The insulin and glucose dynamics are faster than the beta cell dynamics. Mild hyperglycaemia leads to increasing beta cell numbers, but above a threshold of  $250\text{mg/dL}$  blood glucose, beta cell death is greater than cell division. Additional terms (not shown) include and non-functional beta cells ( $\beta_f$  and  $\beta_{nf}$ ), activated macrophage, pathogenic T cells, insulin resistance, mTOR levels and beta cell antigenic protein concentrations [54]. The distinction between beta cells into functioning and non-functioning cells allows to take into account for the reduction and exhaustion of insulin produced by the beta cells. Although the preliminary outcomes of the DIRECT study suggests that beta cells can be restored to normal function through the removal of excess fat in the cells [55, 56], we have not taken into account the recovery of the pancreatic function. Inflammation is key in diabetes, and the interaction between inflammation and metabolism can be considered a key homeostatic mechanism [57]. The model considers both the effect of exercise and dietary [58]. This model was analysed using sensitivity analysis and investigation to determine its properties (not shown). Sensitivity analyses are commonly used in inverse modelling to determine how significant each parameter is to the output variables of the system. A local analysis describes the sensitivity relative to point estimates of the parameters whereas a global analysis examines the entire parameter distribution.

$$\frac{dG}{dt} = R_0 - G \left( E_{G0} + \overbrace{S_I \frac{I}{I_R + i}}^{\text{effect of insulin resistance}} \right) + \overbrace{R_1 H_m(t)}^{\text{diet}} - \overbrace{R_2 H_w(t)}^{\text{workouts}} \quad (6)$$

$$\frac{dI}{dt} = \sigma \overbrace{\frac{\beta_f G^2}{\alpha + G^2}}^{\text{effect of glucose}} - kI \quad (7)$$

$$\frac{d\beta_f}{dt} = -r_0 + r_1 G - r_2 G^2 \beta \quad (8)$$

$$\frac{dI_R}{dt} = -i_0 I_R + \overbrace{mCyt}^{\text{pro-inflammatory cytokines}} + qI \quad (9)$$

where  $G$  is the glucose concentration,  $I$  is Insulin concentration,  $\beta_f$  functioning  $\beta$ -cells,  $I_R$  insulin resistance, and  $Cyt$  is the concentration of pro-inflammatory cytokines [59, 60, 61].  $H_m$  and  $H_w$  are two step functions describing glucose intake during meals and glucose consumption during workouts respectively:

$$H_m = \sum_i g_{m,i} s_{m,i} I_{t_{m,i}(1+\Delta_m)}(t) \quad (10)$$

$$H_w = \sum_i z_{w,i} I_{t_{w,i}(1+\Delta_w)}(t) \quad (11)$$

where  $g_m$  is the glycemic load,  $s_m$  the carbohydrate serving, and  $t_m$  the meal starting time;  $z_w$  the number of burned calories and  $t_w$  the workout starting time;  $I_{t_{m,i}(1+\Delta_m)}(t)$  and  $I_{t_{w,i}(1+\Delta_w)}(t)$  are indicator functions.

Here we consider progressive alteration of arterial stiffness and hypertension in diabetic patients. It is noteworthy that low chronic inflammation related to metabolic active abdominal obesity (abnormal secretion of adipokines and cytokines like TNF-alfa and interferon) and the impaired immune-response to infection (abnormal cytokine profile and T-cell and macrophage activation) cause an increased risk for COVID-19 severity. Diabetic patients are frailer with respect to normal population against COVID-19 multi-organ and multi-process disruption.



### 5.3 Circulatory system model

Circulatory system models are used to describe blood flow, volume, and pressure dynamics. Equations 20-116 illustrate a simplified open-loop cardiovascular model composed of five components: heart (20-40), systemic circulation (41-75), pulmonary circulation (76-89), coronary circulation (90-105), and baroreceptors (106-110). Equations have been derived from the open-loop circulatory model proposed in [12]. The heart model is composed of four sections (chambers) corresponding to right atrium, right ventricle, left atrium, and left ventricle. Each chamber is modeled as a bellows pump comprised of a one-way valve (pulmonary, tricuspid, mitral, and aortic) and a time-varying elastance (Eq. 27) controlling blood outflow [62, 63]. Blood inflow is passive. The systemic circulation has been modeled with seven vascular segments: proximal aorta, distal aorta, arteries, arterioles, capillaries, veins, and the vena cava. Each vessel has been designed using a resistance element reflecting the impact on blood flow reduction and a compliance element indicating the tendency of arteries and veins to stretch in response to pressure. High-frequency effects caused by wave reflections at great arterial bifurcations (distal and proximal aorta) are modeled with inertance elements. Arterioles, veins and vena cava have unique nonlinear PV relationships as described in [64] (see Eqs. 49-51, 53, and 41). The pulmonary circulation is composed of five vascular segments: proximal and distal pulmonary artery, small arteries, capillaries, and veins. Wave reflections in the proximal and distal pulmonary arteries are modeled with inertance elements. The coronary circulation model consists of four segments: epicardial and intramural arteries, coronary capillaries, and coronary veins. Following [12], large and small artery and vein segments proposed in [65] have been condensed into intramural arteries and coronary veins, respectively. Baroreceptors are special sensory neurons that are excited by a stretch in the carotid sinus and aortic arch vessels. Their feedback is processed by the brain in order to maintain proper blood pressure. Baroreceptors' firing frequency to the brain has been modeled as a second-order response to the aortic pressure change [66, 64]. The second-order differential equation has been rewritten into two first order equations in order to make it compatible with common Python solvers (Eqs. 108 and 109).

Circulatory system parameters and initial conditions have been reported in table 7.

### 5.4 Stiffness model

The complexity underlying multifactorial diseases requires the introduction of computational systems representing multi-organ and inter-process communication. To this aim, we propose a mathematical model describing the impact of comorbidities on the circulatory system. Several factors influencing blood pressure and arterial stiffness have been modeled including: diabetes, renal impairments, viral infections, lifestyle and ageing.

Ageing affects the circulatory system in multiple ways. Baroreceptors' feedback and pathways to the heart's pacemaker system decrease their efficiency over time. Heart muscle cells tend to degenerate and its walls get thicker slowing down the time the heart takes to fill with blood increasing pressure on the vessels. Besides, blood vessels show a decreased performance, since arteries tend to narrow and become more rigid.

Glucose concentration affects the renin-angiotensin-aldosterone pathway as it controls the concentration and activity of Renin, ACE, and AT1R. AT1R activity is strongly related to vasoconstriction, hypertension, and inflammatory response. Hence, arterial stiffness gets even worse increasing the risks of clogged arteries and strokes. Besides, SARS-CoV-2 strongly bind to ACE2 decreasing its availability and impacting downstream RAS pathways regulating blood pressure. Lower levels of available ACE2 reduce the concentration of ANG-(1-7), the endogenous ligand for the G protein-coupled receptor MAS, a receptor associated with cardiac, renal, and cerebral protective responses. Hence, vasoprotection and hypotension feedbacks deteriorate increasing inflammatory response and pressure on blood vessels.

The combined effect of comorbidities and ageing factors on arterial stiffness and inflammation may lead to critical circulatory conditions and fibrosis. High glucose concentrations strengthen RAS hypertension feedbacks and lower blood vessels' lumen, especially on capillaries, arterioles, and venules. By affecting blood pressure regulation pathways, SARS-CoV-2 infections may impair vasoprotection regulation by the RAS endangering the whole circulatory system with disruptive repercussions among the elderly. The combination of all such factors may lead to acute diseases such as thrombophlebitis, cardiomyopathy, myocardial infarction, pulmonary embolism, heart failure, and eventually to patients' death.

The diabetic model (Sec. 5.2) accounts both for hyperglycemic conditions and lifestyle habits. After lunch and dinner, glucose concentration in blood vessels peaks, while it is scaled down by insulin or physical exercise. The RAS model (Sec. 5.1) has been used to simulate peptides' and drug concentration dynamics taking into account glucose concentration, ACE inhibitor treatments, renal conditions, and viral infections binding to ACE2 (such as COVID19). Abnormal ACE2 activity ( $k_{ACE2} - k_{ACE2,0}$ ) has been assumed as proportional to SARS-CoV-2 infectivity (see Eq. 5). ACEi or ARB treatments could also increase ACE2 abundance and thus enhance viral entry [45]. In case of severe renal conditions, only a fraction of drug diacid is expelled before the subsequent administration (see Eq. 1 and Fig. 4). The

drug surplus left inside the body may reinforce inflammation. Overall, the inflammatory response has been modeled as a function of all such contributions:

$$\frac{dIR}{dt} = \overbrace{k_{SARS}(k_{ACE2} - k_{ACE2,0})}^{\text{viral infection}} + \overbrace{k_D[Drug]}^{\text{drug treatment}} + \overbrace{k_G G}^{\text{glucose}} - \overbrace{k_{eff} IR}^{\text{anti-inflammatory response}} \quad (12)$$

where  $k_{SARS}$  represents SARS-CoV-2 affinity with ACE2,  $k_D$  the inflammation rate due to ACEi surplus,  $k_G$  the inflammation rate due to glucose surplus, and  $k_{eff}$  the anti-inflammatory response rate.

One of the main processes associated with arterial stiffness occurring during ageing is DNA methylation, consisting in the addition of methyl groups to the DNA molecule which may modify the activity of a DNA segment without changing the sequence. DNA methylation has been modeled as a linear function of the age  $A$  [27]:

$$\alpha_{MET} = \beta_0 - \beta_1 A \quad \beta_{0,1} \geq 0 \quad (13)$$

As a result, blood vessels' compliance parameters have been reduced by a factor accounting for the combined effect of inflammation (Eq. 12) and ageing (Eq. 13):

$$\hat{C}_i = \overbrace{\alpha_{MET} \left(1 - \frac{IR}{100}\right)}^{\text{stiffness}} C_i \quad (14)$$

where  $C_i$  is the compliance of the blood vessel  $i$  for a young healthy individual and  $\hat{C}_i$  is the reduced compliance. The circulatory model (Sec. 5.3) has been used to simulate blood pressure dynamics in critical vessels where blood pressure spikes may lead to acute diseases.

## 6 Experiments

The models presented in Section 5 have been solved to analyze the effects of comorbidities like diabetes, renal impairment, and viral infections affecting the circulatory system. Table 2 reports the set of experimental conditions that have been analysed. Five Computational patients have been created corresponding to different physiological states. These scenarios have been further stratified by the age of the Computational patient, given that arterial stiffness has been modeled as a function of the increased DNA methylation during ageing. Drug concentrations (Fig. 4), inflammation levels, and blood pressure dynamics in lungs' vessels (Fig. 5) in comorbid conditions have been compared to the dynamics obtained in healthy states or using ACE inhibitor treatments.

Table 2: Computational patients' conditions used for the simulations. The diabetic and the RAS models do not depend on patient's age. Lifestyle habits have been set as three meals and one light workout session in the afternoon for all patients.

Label	Age	Description
H	20	Healthy individual
D	-	Diabetic individual
R	-	Individual with renal impairment
C+T	70	Individual with comorbid conditions (diabetes + renal impairment) treated with ACEi
V	70	Individual with COVID19
C+V	70	Individual with comorbid conditions and COVID19
C+V+T	70	Individual with comorbid conditions and COVID19 treated with ACEi

The RAS model has been simulated for constant glucose cases using the daily glucose peak predicted by the diabetic model right after the main meals. Glucose concentration ranged between the extremes of normal glucose at 6 – 7 mmol/L (corresponding to 108 – 125 ml/dl) and high glucose at 10 – 11 mmol/L (corresponding to 180 – 200 ml/dl) based on experimental studies [67, 68, 69]. The time window of the RAS simulations has been set to five

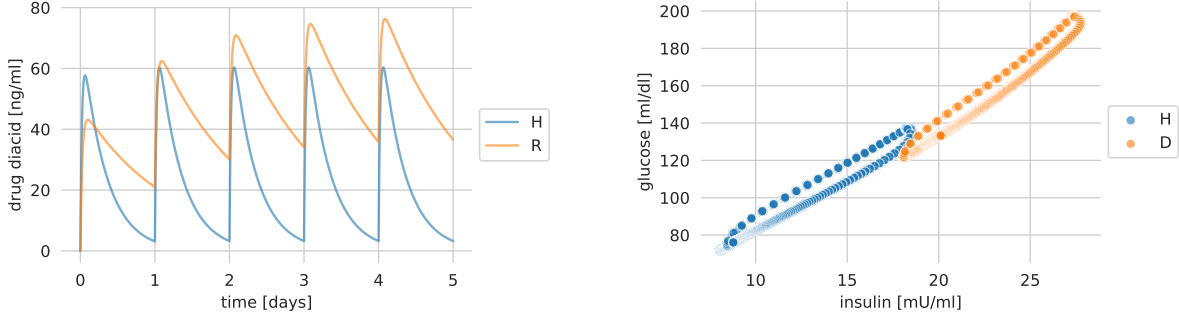


Figure 4: Drug concentration for healthy individuals and patients with renal impairments (**left**). Glucose-insulin phase space for healthy and diabetic individuals (**right**).

days, corresponding to five daily ACEi administrations [44]. The simulation results have been used to compute arterial stiffness and to reduce compliance parameters of blood vessels in the open-loop circulatory model. In the following simulations the arterial blood pressure (ABP) signal used in [12] has been used instead of personalised clinical measurements.

Fig. 4 shows the dynamics of the concentration of ACEi and glucose-insulin dynamics over the first five days of treatment. Due to renal impairment, the Computational patient was not able to expel the drug dose before the next administration. The inflammatory response and the corresponding blood pressure dynamics in lungs' vessels are shown in Fig. 5. Comorbid conditions tend to increase blood pressure variability in all scenarios. However, as arterial stiffness grows with the age of the Computational patient, the variability increases as well, possibly leading to irreversible deterioration of blood vessels' walls. ACEi treatments may help in reducing inflammation levels, but may not be sufficient to recover healthy blood pressures. One of the most serious effects illustrated by simulations consists of an increased mean value of blood pressure and blood pressure variability especially on small pulmonary vessels and capillaries (see Fig. 5), increasing the risk of clogged arteries, fibrosis, and strokes. Besides, experimental results shows how variables fluctuations over time may change and present different shapes especially on small vessels. In Computational patients with comorbidities blood pressure dynamics in pulmonary capillaries exhibit higher mean values and variability, but beat frequencies can be observed as well.

## 6.1 COVID19

The mortality statistics remarks the relevance of deeper analysis on multi-factorial diseases in fighting the COVID-19 pandemia [9]. Underlying morbidities such as cardiovascular disease, kidney disease, T2D or tumours have been observed in patients with severe infection, especially among the elderly [10]. By affecting blood pressure regulation pathways, SARS-CoV-2 infections may impair vasoprotection regulation endangering the whole circulatory system with severe repercussions. By taking advantage of our composable framework, experimental results offer an overview on how the combination of multiple diseases with SARS-CoV-2 may lead to acute conditions. Fig. 5 clearly shows how the Computational patient with comorbidities and SARS-CoV-2 has higher risk of pulmonary vessels' deterioration.

It is noteworthy that autopsy-based findings have evidenciated a variety of damages caused by COVID-19 infection, among which extensive coagulopathy, acquired thrombophilia and endothelial cell death [70]. Here we consider the sole effect on blood pressure.

## 7 Discussion

The modularity and composability of different available mechanistic and phenomenological models presents the challenge to define a mathematical framework connecting different systems' descriptions, their dynamics, and constraints. Let's imagine to put together a model based on ODEs and a model in terms of a discrete space discrete time Markov chain. This has then to be done in the light of behavioral properties that can be sets of trajectories or measures on the trajectory space (typically those learned from data with statistical methods). Cell-level models (using ODEs, delay differential equations, DDE, or agents) need to be systematically scaled up to the tissue level; for the multiple timescale problems, the challenge is to obtain a model order reduction, i.e. to abandon high dimensional bioengineering systems in favour of simpler effective mathematical models. The tissue level could be modeled using PDE or cellular Potts model which may provide better representation for detailed and heterogeneous cell-cell, cell-tissue, cell-matrix

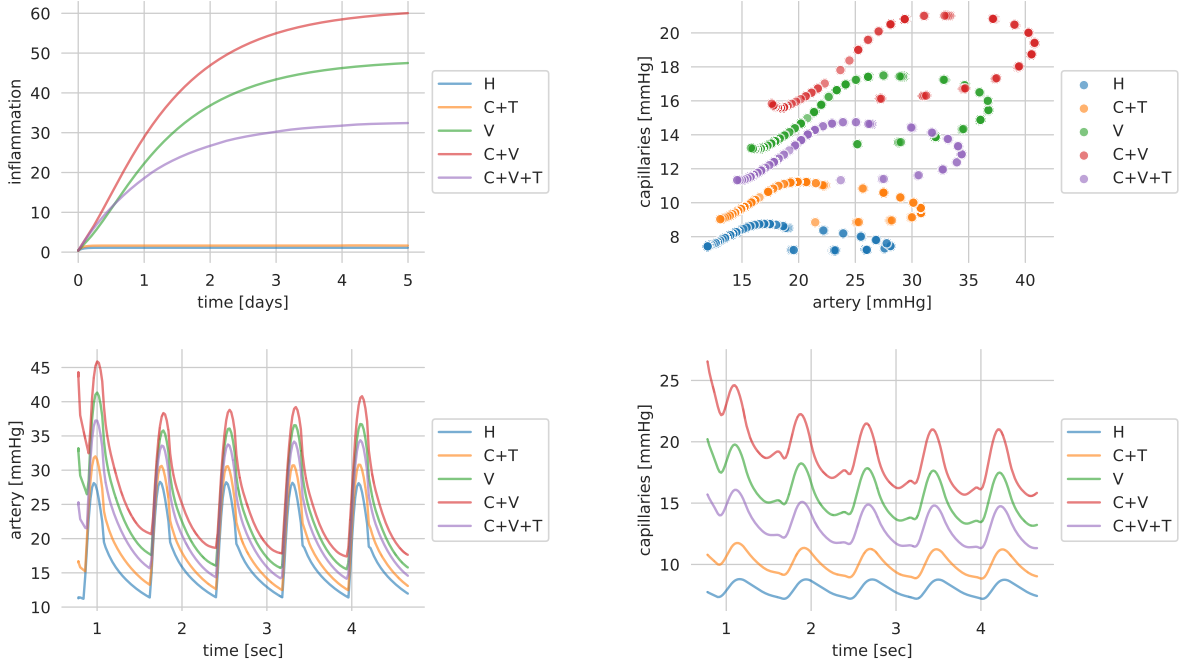


Figure 5: Inflammation scores (**top-left**, see Eq. 12), the corresponding lungs' pressures phase space (**top-right**) and dynamics over time (**bottom**)

interaction cases. Integrative models, could be made by single scale models, describing the biological process at different characteristic space-time scales, and scale bridging models, which define how the component models are coupled to each other. While at the tissue level, physical quantities usually vary across space and time, in a continuous fashion, and can be thus represented using systems of PDE [71].

### 7.1 Emerging properties of variances from model composability

Many physiological variables have a circadian trend; sometimes also a seasonal one. For example blood pressure decreases during sleep and shows a sharp uprise at the time of awakening. This early morning variation is often concurrent with an increase of acute myocardial infarction, sudden cardiac death, and stroke. [72]. Common clinical parameters such as diastolic and systolic blood pressure, heart patterns, blood cell counts are usually evaluated as averages. Little importance is given to higher moments such as variances during the day or during a longer interval of time. The lack of continuous measures for most of the quantities has generated a medical practice that disregard of unobserved or partially observed data. Some authors identified a disease and age-related loss of complex variability in multiple physiologic processes including cardiovascular control, pulsatile hormone release, and ecg data [73, 74]. Our composable model reveals interesting patterns, particularly fluctuations in blood pressure, particularly during COVID acute infection when the diabetic model is coupled with the RAS and the cardiovascular models. We believe that the use of extensive models could enable to understand concurrent patterns of alteration in different districts.

### 7.2 How such Computational patient model could be deployed and further developed

Computational Patient will benefit from using machine learning and data analysis of large amount of data such for instance that obtained from UK Biobank as modeling will have a truly catalytic effect in synergy with machine learning. The Computational patient model requires adequate artificial intelligence support to generate diagnosis and validate its correctness. A decision-making process could be based on the development of a personalised statistics of Changes in Health, End-stage disease, and Signs and Symptoms [75]. This ideally would develop through monitoring of the individualized response to therapeutic interventions, in addition to changes in risk profile. One aspect is a dedicated CHES (“Changes in Health, End-stage disease, and Signs and Symptoms”) (CHES) scale based on all the variables and observable considered by the model(s) [75, 76]. It will act as a Personalised Patient simulator and will

draw temporal trajectories of disease and comorbidities progression. The trajectories will change with drug regimen, medical intervention, and lifestyle changes.

Any data used will be anonymised or de-identified using ad hoc software (see for instance [77]) and we will follow the FAIR principle (Findable, Accessible, Interoperable, Reusable) and the GDPR regulation. One meaningful approach to extract useful indication is to use a clinical decision support system such as the one described in [78] which incorporates medical experience, research results and personal judgement. We believe the Computational patient models to be in a research only state and therefore we do not make further integrations.

The future foreseen is that AI will assist our health and disease conditions in a more effective way than nowadays: a medical check up will be supported by well-tuned artificial intelligence and patient-based modeling. At the clinical level, computer-aided therapies and treatments will develop into intervention strategies undertaken under acute disease conditions or due to external factors (infections) to contrast cascade effects. In non acute states, predictive inference will propose prevention plans for comorbidity management, particularly in presence of multiple therapies.

Therefore this approach is meaningful in perspective of a computational medicine characterised by a close coupling between bioinformatics, clinical measures and modeling prediction and perhaps remote patient monitoring.

## 8 Conclusion

Computational scientists and bioengineers' vision is a framework of methods and technologies that, once established, will make it possible to investigate the human body as a whole. It calls for a total transformation in the way healthcare currently works and is delivered to patients. Underpinning this transformation is substantial technological innovation with a requirement for deeper trans-disciplinary research, improved IT infrastructure, better communication, large volumes of high quality data and machine learning and modeling tools. Machine learning could be automatised (i.e. autoML) and models should be modular so to be organised to answer specific and personalised medical questions. Simulations are increasingly regarded as valuable tools in a number of aspects of medical practice including lifestyle changes, surgical planning and medical interventions. The idea is that cross-modality data is obtained for the patient and machine learning techniques estimate parameters to be input into modeling framework. We believe that a deeper understanding and practice of modeling in medicine will produce better investigation of complex biological processes, and even new ideas and better feedback into medicine. Finally, computational models are cheap and this will make possible to predict drugs interaction and to make better use of generic drugs. In this sense the personalised model will become a product associated with the drug.

### 8.1 Disclaimer

**The computational tool has not been validated and should not be used for clinical purposes.**

To enable code reuse, the Python code for the mathematical models including parameter values and documentation is freely available under Apache 2.0 Public License from a GitHub repository [19]. Unless required by applicable law or agreed to in writing, software is distributed on an "as is" basis, without warranties or conditions of any kind, either express or implied.

## 9 Acknowledgement

The authors have received funding from the European Union's Horizon 2020 research and innovation programme under grant agreement No 848077. We thank Gianluca Ascolani, Rachel Clark, Annalisa Occhipinti, Stefan Stojanovic for suggestions.

## References

- [1] Gianluca Ascolani, Annalisa Occhipinti, and Pietro Liò. Modelling circulating tumour cells for personalised survival prediction in metastatic breast cancer. *PLOS Computational Biology*, 11(5):e1004199, May 2015.
- [2] E. Giampieri, D. Remondini, L. de Oliveira, G. Castellani, and P. Lió. Stochastic analysis of a miRNA–protein toggle switch. *Molecular BioSystems*, 7(10):2796, 2011.
- [3] Joëlle Despeyroux, Amy Felty, Pietro Liò, and Carlos Olarte. A logical framework for modelling breast cancer progression. In *Molecular Logic and Computational Synthetic Biology*, pages 121–141. Springer International Publishing, 2019.



- [4] Ezio Bartocci and Pietro Lió. Computational modeling, formal analysis, and tools for systems biology. *PLoS computational biology*, 12(1), 2016.
- [5] Ezio Bartocci, Pietro Lió, Emanuela Merelli, and Nicola Paoletti. Multiple verification in complex biological systems: the bone remodelling case study. In *Transactions on Computational Systems Biology XIV*, pages 53–76. Springer, 2012.
- [6] Sandip Ray, Markus Britschgi, Charles Herbert, Yoshiko Takeda-Uchimura, Adam Boxer, Kaj Blennow, Leah F Friedman, Douglas R Galasko, Marek Jutel, Anna Karydas, et al. Classification and prediction of clinical alzheimer’s diagnosis based on plasma signaling proteins. *Nature medicine*, 13(11):1359–1362, 2007.
- [7] Nobuyuki Sudo, Yoichi Chida, Yuji Aiba, Junko Sonoda, Naomi Oyama, Xiao-Nian Yu, Chiharu Kubo, and Yasuhiro Koga. Postnatal microbial colonization programs the hypothalamic-pituitary-adrenal system for stress response in mice. *The Journal of Physiology*, 558(1):263–275, June 2004.
- [8] Sirisha Achanta, Jonathan Gorky, Clara Leung, Alison Moss, Shaina Robbins, Leonard Eisenman, Jin Chen, Susan Tappan, Maci Heal, Navid Farahani, Todd Huffman, Steve England, Zixi (Jack) Cheng, Rajanikanth Vadigepalli, and James S. Schwaber. A comprehensive integrated anatomical and molecular atlas of rat intrinsic cardiac nervous system. *iScience*, page 101140, May 2020.
- [9] Bertrand Cariou, , Samy Hadjadj, Matthieu Wargny, Matthieu Pichelin, Abdallah Al-Salameh, Ingrid Allix, Coralie Amadou, Gwénaëlle Arnault, Florence Baudoux, Bernard Bauduceau, Sophie Borot, Muriel Bourgeon-Ghittori, Olivier Bourron, David Boutoille, France Cazenave-Roblot, Claude Chaumeil, Emmanuel Cosson, Sandrine Coudol, Patrice Darmon, Emmanuel Disse, Amélie Ducet-Boiffard, Bénédicte Gaborit, Michael Joubert, Véronique Kerlan, Bruno Laviolle, Lucien Marchand, Laurent Meyer, Louis Potier, Gaëtan Prevost, Jean-Pierre Riveline, René Robert, Pierre-Jean Saulnier, Ariane Sultan, Jean-François Thébaut, Charles Thivolet, Blandine Tramunt, Camille Vatier, Ronan Roussel, Jean-François Gautier, and Pierre Gourdy. Phenotypic characteristics and prognosis of inpatients with COVID-19 and diabetes: the CORONADO study. *Diabetologia*, May 2020.
- [10] Tianbing Wang, Zhe Du, Fengxue Zhu, Zhaolong Cao, Youzhong An, Yan Gao, and Baoguo Jiang. Comorbidities and multi-organ injuries in the treatment of COVID-19. *The Lancet*, 395(10228):e52, March 2020.
- [11] Safiya Richardson, Jamie S. Hirsch, Mangala Narasimhan, James M. Crawford, Thomas McGinn, Karina W. Davidson, Douglas P. Barnaby, Lance B. Becker, John D. Chelico, Stuart L. Cohen, Jennifer Cookingham, Kevin Coppa, Michael A. Diefenbach, Andrew J. Dominello, Joan Duer-Hefele, Louise Falzon, Jordan Gitlin, Negin Hajizadeh, Tiffany G. Harvin, David A. Hirschwerk, Eun Ji Kim, Zachary M. Kozel, Lyndonna M. Marrast, Jazmin N. Mogavero, Gabrielle A. Osorio, Michael Qiu, and Theodoros P. Zanos and. Presenting characteristics, comorbidities, and outcomes among 5700 patients hospitalized with COVID-19 in the new york city area. *JAMA*, April 2020.
- [12] Maxwell Lewis Neal and James B Bassingthwaite. Subject-specific model estimation of cardiac output and blood volume during hemorrhage. *Cardiovascular engineering*, 7(3):97–120, 2007.
- [13] B Topp, K Promislow, G Devries, RM Miuraa, and DT Finegood. A Model of  $\beta$ -cell mass, insulin and glucose kinetics: Pathways to diabetes. *J. theor. Biol.*, 206:605–609, 2000. doi:10.1006/jtbi.2000.2150.
- [14] Minu R Pilvankar, Hui Ling Yong, and Ashlee N Ford Versypt. A glucose-dependent pharmacokinetic/pharmacodynamic model of ace inhibition in kidney cells. *Processes*, 7(3):131, 2019.
- [15] Peter Hunter, Peter Robbins, and Denis Noble. The iups human physiome project. *Pflügers Archiv*, 445(1):1–9, 2002.
- [16] S Van Sint Jan, M Viceconti, and G Clapworthy. The europsiome: towards an infrastructure for a more integrated research. *Journal of biomechanics*, 40:S282, 2007.
- [17] Jeremy Gunawardena. Models in systems biology: the parameter problem and the meanings of robustness. *Elements of Computational Systems Biology*. New Jersey: John Wiley and Sons, pages 21–48, 2010.
- [18] Peter Cull. *The Sourcebook of medical illustration: over 900 anatomical, medical, and scientific illustrations available for general re-use and adaptation free of normal copyright restrictions*. Parthenon Publishing, 1989.
- [19] Pietro Barbiero and Pietro Lió. <https://github.com/pietrobarbiero/computational-patient>.
- [20] Alan C Hindmarsh. Odepack, a systematized collection of ode solvers. *Scientific computing*, pages 55–64, 1983.
- [21] Linda Petzold. Automatic selection of methods for solving stiff and nonstiff systems of ordinary differential equations. *SIAM journal on scientific and statistical computing*, 4(1):136–148, 1983.
- [22] Fernando Pérez, HP Langtangen, and R LeVeque. Python for scientific computing. In *SIAM Conference on Computational Science and Engineering*, volume 42, 2009.



- [23] Katherine Howell, Henry Ooi, Rob Preston, and Paul McLoughlin. Structural basis of hypoxic pulmonary hypertension: the modifying effect of chronic hypercapnia. *Experimental Physiology*, 89(1):66–72, December 2003.
- [24] Bum Joon Kim, Sun U. Kwon, Dalia Wajsbrot, Jaseong Koo, Jong Moo Park, and Barrett W. Jeffers. Relationship of inter-individual blood pressure variability and the risk for recurrent stroke. *Journal of the American Heart Association*, 7(24), December 2018.
- [25] Y Tao, J Xu, B Song, X Xie, H Gu, Q Liu, L Zhao, Y Wang, Y Xu, and Y Wang. Short-term blood pressure variability and long-term blood pressure variability: which one is a reliable predictor for recurrent stroke. *Journal of Human Hypertension*, 31(9):568–573, April 2017.
- [26] Igor A. Fernandes, Marcos P. Rocha, Monique O. Campos, João D. Mattos, Daniel E. Mansur, Helena N. M. Rocha, Paulo A. C. Terra, Vinícius P. Garcia, Natália G. Rocha, Niels H. Secher, and Antonio C. L. Nóbrega. Reduced arterial vasodilatation in response to hypoxia impairs cerebral and peripheral oxygen delivery in hypertensive men. *The Journal of Physiology*, 596(7):1167–1179, February 2018.
- [27] Wen Wen, Rong Luo, Xiaojing Tang, Lan Tang, Hunter X. Huang, Xiaoyan Wen, Shan Hu, and Bin Peng. Age-related progression of arterial stiffness and its elevated positive association with blood pressure in healthy people. *Atherosclerosis*, 238(1):147–152, January 2015.
- [28] Michael F. O’Rourke and Wilmer W. Nichols. Aortic diameter, aortic stiffness, and wave reflection increase with age and isolated systolic hypertension. *Hypertension*, 45(4):652–658, April 2005.
- [29] Gary F. Mitchell, Shih-Jen Hwang, Ramachandran S. Vasani, Martin G. Larson, Michael J. Pencina, Naomi M. Hamburg, Joseph A. Vita, Daniel Levy, and Emelia J. Benjamin. Arterial stiffness and cardiovascular events. *Circulation*, 121(4):505–511, February 2010.
- [30] Sripal Bangalore, David J. Maron, Sean M. O’Brien, Jerome L. Fleg, Evgeny I. Kretov, Carlo Briguori, Upendra Kaul, Harmony R. Reynolds, Tomasz Mazurek, Mandeep S. Sidhu, Jeffrey S. Berger, Roy O. Mathew, Olga Bockeria, Samuel Broderick, Radoslaw Pracon, Charles A. Herzog, Zhen Huang, Gregg W. Stone, William E. Boden, Jonathan D. Newman, Ziad A. Ali, Daniel B. Mark, John A. Spertus, Karen P. Alexander, Bernard R. Chaitman, Glenn M. Chertow, and Judith S. Hochman. Management of coronary disease in patients with advanced kidney disease. *New England Journal of Medicine*, 382(17):1608–1618, April 2020.
- [31] Donald Clark, Stephen J. Nicholls, Julie St John, Mohamed B. Elshazly, Haitham M. Ahmed, Haitham Khraishah, Steven E. Nissen, and Rishi Puri. Visit-to-visit blood pressure variability, coronary atheroma progression, and clinical outcomes. *JAMA Cardiology*, 4(5):437, May 2019.
- [32] Tokuhisa Uejima, Frank D. Dunstan, Eloisa Arbustini, Krystyna Łoboz-Grudzień, Alun D. Hughes, Scipione Carerj, Valentina Favalli, Francesco Antonini-Canterin, Olga Vríz, Dragos Vinereanu, Jose L. Zamorano, Bogdan A. Popescu, Arturo Evangelista, Patrizio Lancellotti, Georges Lefthériotis, Michaela Kozakova, Carlo Palombo, and Alan G. Fraser. Age-specific reference values for carotid arterial stiffness estimated by ultrasonic wall tracking. *Journal of Human Hypertension*, 34(3):214–222, August 2019.
- [33] Iram Faqir Muhammad, Yan Borné, Gerd Östling, Cecilia Kennbäck, Mikael Gottsäter, Margaretha Persson, Peter M. Nilsson, and Gunnar Engström. Arterial stiffness and incidence of diabetes: A population-based cohort study. *Diabetes Care*, 40(12):1739–1745, September 2017.
- [34] Min Xu, Ya Huang, Lan Xie, Kui Peng, Lin Ding, Lin Lin, Po Wang, Mingli Hao, Yuhong Chen, Yimin Sun, Lu Qi, Weiqing Wang, Guang Ning, and Yufang Bi. Diabetes and risk of arterial stiffness: A mendelian randomization analysis. *Diabetes*, 65(6):1731–1740, March 2016.
- [35] Wei Gan, Fiona Bragg, Robin G. Walters, Iona Y. Millwood, Kuang Lin, Yiping Chen, Yu Guo, Julien Vaucher, Zheng Bian, Derrick Bennett, Jun Lv, Canqing Yu, Anubha Mahajan, Robert J. Clarke, Liming Li, Michael V. Holmes, Mark I. McCarthy, and Zhengming Chen. Genetic predisposition to type 2 diabetes and risk of subclinical atherosclerosis and cardiovascular diseases among 160, 000 chinese adults. *Diabetes*, 68(11):2155–2164, August 2019.
- [36] James M. Eales, Simon P.R. Romaine, Fadi J. Charchar, and Maciej Tomaszewski. A multi-omics glimpse into the biology of arterial stiffness. *Journal of Hypertension*, 34(1):32–35, January 2016.
- [37] Claudio Franceschi, Massimiliano Bonafè, Silvana Valensin, Fabiola Olivieri, Maria De Luca, Enzo Ottaviani, and Giovanna De Benedictis. Inflamm-aging: an evolutionary perspective on immunosenescence. *Annals of the new York Academy of Sciences*, 908(1):244–254, 2000.
- [38] Irene Maeve Rea, David S. Gibson, Victoria McGilligan, Susan E. McNerlan, H. Denis Alexander, and Owen A. Ross. Age and age-related diseases: Role of inflammation triggers and cytokines. *Frontiers in Immunology*, 9, April 2018.

- [39] Sungha Park and Edward G. Lakatta. Role of inflammation in the pathogenesis of arterial stiffness. *Yonsei Medical Journal*, 53(2):258, 2012.
- [40] K. M. Madden, C. Lockhart, D. Cuff, T. F. Potter, and G. S. Meneilly. Short-term aerobic exercise reduces arterial stiffness in older adults with type 2 diabetes, hypertension, and hypercholesterolemia. *Diabetes Care*, 32(8):1531–1535, June 2009.
- [41] John H Fountain and Sarah L Lappin. Physiology, renin angiotensin system. In *StatPearls [Internet]*. StatPearls Publishing, 2019.
- [42] Keiji Kuba, Yumiko Imai, Takayo Ohto-Nakanishi, and Josef M Penninger. Trilogy of ace2: A peptidase in the renin–angiotensin system, a sars receptor, and a partner for amino acid transporters. *Pharmacology & therapeutics*, 128(1):119–128, 2010.
- [43] Mariela M Gironacci, Hugo P Adamo, Gerardo Corradi, Robson A Santos, Pablo Ortiz, and Oscar A Carretero. Angiotensin (1-7) induces mas receptor internalization. *Hypertension*, 58(2):176–181, 2011.
- [44] Mohammad Amin Zaman, Suzanne Oparil, and David A Calhoun. Drugs targeting the renin–angiotensin–aldosterone system. *Nature reviews Drug discovery*, 1(8):621–636, 2002.
- [45] Andrew M South, Laurie Tomlinson, Daniel Edmonston, Swapnil Hiremath, and Matthew A Sparks. Controversies of renin–angiotensin system inhibition during the covid-19 pandemic. *Nature Reviews Nephrology*, pages 1–3, 2020.
- [46] Ashlee N Ford Versypt, Grace K Harrell, and Alexandra N McPeak. A pharmacokinetic/pharmacodynamic model of ace inhibition of the renin-angiotensin system for normal and impaired renal function. *Computers & Chemical Engineering*, 104:311–322, 2017.
- [47] James P Byers and Jeffrey G Sarver. Pharmacokinetic modeling. In *Pharmacology*, pages 201–277. Elsevier, 2009.
- [48] Minu R Pilvankar, Michele A Higgins, and Ashlee N Ford Versypt. Mathematical model for glucose dependence of the local renin–angiotensin system in podocytes. *Bulletin of mathematical biology*, 80(4):880–905, 2018.
- [49] Arthur Lo, Jennifer Beh, Hector De Leon, Melissa K Hallow, Ramprasad Ramakrishna, Manoj Rodrigo, Anamika Sarkar, Ramesh Sarangapani, and Anna Georgieva. Using a systems biology approach to explore hypotheses underlying clinical diversity of the renin angiotensin system and the response to antihypertensive therapies. In *Clinical Trial Simulations*, pages 457–482. Springer, 2011.
- [50] S. Sharif, F. L. J. Visseren, W. Spiering, P. A. Jong, M. L. Bots, and J. Westerink and. Arterial stiffness as a risk factor for cardiovascular events and all-cause mortality in people with type 2 diabetes. *Diabetic Medicine*, 36(9):1125–1132, April 2019.
- [51] Rafael de Oliveira Alvim, Paulo Caleb Junior Lima Santos, Mariane Musso, Roberto de Sá Cunha, José Krieger, José Mill, and Alexandre Pereira. Impact of diabetes mellitus on arterial stiffness in a representative sample of an urban brazilian population. *Diabetology & Metabolic Syndrome*, 5(1):45, 2013.
- [52] Yao Lu, Raimund Pechlaner, Jingjing Cai, Hong Yuan, Zhijun Huang, Guoping Yang, Jiangang Wang, Zhiheng Chen, Stefan Kiechl, and Qingbo Xu. Trajectories of age-related arterial stiffness in chinese men and women. *Journal of the American College of Cardiology*, 75(8):870–880, March 2020.
- [53] Alejandro Diaz, Matías Tringler, Sandra Wray, Agustín J. Ramirez, and Edmundo I. Cabrera Fischer. The effects of age on pulse wave velocity in untreated hypertension. *The Journal of Clinical Hypertension*, 20(2):258–265, December 2017.
- [54] K. Kodama, M. Horikoshi, K. Toda, S. Yamada, K. Hara, J. Irie, M. Sirota, A. A. Morgan, R. Chen, H. Ohtsu, S. Maeda, T. Kadowaki, and A. J. Butte. Expression-based genome-wide association study links the receptor CD44 in adipose tissue with type 2 diabetes. *Proceedings of the National Academy of Sciences*, 109(18):7049–7054, April 2012.
- [55] Sviatlana V. Zhyzhneuskaya, Ahmad AL-Mrabeh, Alison C. Barnes, Benjamin Aribisala, Kieren G. Hollingsworth, Helen Pilkington, Naveed Sattar, Michael E. Lean, and Roy Taylor. 66-OR: Remission of type 2 diabetes for two years is associated with full recovery of beta-cell functional mass in the diabetes remission clinical trial (DiRECT). *Diabetes*, 68(Supplement 1):66–OR, June 2019.
- [56] Michael EJ Lean, Wilma S Leslie, Alison C Barnes, Naomi Brosnahan, George Thom, Louise McCombie, Carl Peters, Sviatlana Zhyzhneuskaya, Ahmad Al-Mrabeh, Kieren G Hollingsworth, Angela M Rodrigues, Lucia Rehackova, Ashley J Adamson, Falko F Sniehotta, John C Mathers, Hazel M Ross, Yvonne McIlvenna, Renae Stefanetti, Michael Trenell, Paul Welsh, Sharon Kean, Ian Ford, Alex McConnachie, Naveed Sattar, and Roy Taylor. Primary care-led weight management for remission of type 2 diabetes (DiRECT): an open-label, cluster-randomised trial. *The Lancet*, 391(10120):541–551, February 2018.

- [57] Gökhan S. Hotamisligil. Inflammation and metabolic disorders. *Nature*, 444(7121):860–867, December 2006.
- [58] Matthias B Schulze, Kurt Hoffmann, JoAnn E Manson, Walter C Willett, James B Meigs, Cornelia Weikert, Christin Heidemann, Graham A Colditz, and Frank B Hu. Dietary pattern, inflammation, and incidence of type 2 diabetes in women. *The American Journal of Clinical Nutrition*, 82(3):675–684, September 2005.
- [59] DH Solomon, TJ Love, C Canning, and et al. Risk of diabetes among patients with rheumatoid arthritis, psoriatic arthritis and psoriasis. *Ann Rheum Dis.*, 69(12):2114–2117, 2010.
- [60] CC Su, IeC Chen, FN Young, and et al. Risk of diabetes in patients with rheumatoid arthritis: a 12-year retrospective cohort study. *J Rheumatol.*, 40(9):1513–1518, 2013.
- [61] MC Lu, ST Yan, WY Yin, and et al. Risk of rheumatoid arthritis in patients with type 2 diabetes: a nationwide population-based case-control study. *PLoS One*, 9(7):e101528, 2014.
- [62] Vincent C Rideout. *Mathematical and computer modeling of physiological systems*. Prentice Hall Englewood Cliffs, NJ., 1991.
- [63] Thomas Heldt, Eun B Shim, Roger D Kamm, and Roger G Mark. Computational modeling of cardiovascular response to orthostatic stress. *Journal of applied physiology*, 92(3):1239–1254, 2002.
- [64] K Lu, JW Clark Jr, FH Ghorbel, DL Ware, and A Bidani. A human cardiopulmonary system model applied to the analysis of the valsalva maneuver. *American Journal of Physiology-Heart and Circulatory Physiology*, 281(6):H2661–H2679, 2001.
- [65] Daniel Zinemanas, Rafael Beyar, and Samuel Sideman. Relating mechanics, blood flow and mass transport in the cardiac muscle. *International journal of heat and mass transfer*, 37:191–205, 1994.
- [66] M Di Rienzo et al. Circulatory model of baro-and cardio-pulmonary reflexes. *Blood Pressure and Heart Rate Variability: Computer Analysis, Modelling and Clinical Applications*, 4:56, 1993.
- [67] Raghu V Durvasula and Stuart J Shankland. Activation of a local renin angiotensin system in podocytes by glucose. *American Journal of Physiology-Renal Physiology*, 294(4):F830–F839, 2008.
- [68] Benito Yard, Yuxi Feng, Hanno Keller, Christa Mall, and Fokko van der Woude. Influence of high glucose concentrations on the expression of glycosaminoglycans and n-deacetylase/n-sulphotransferase mrna in cultured skin fibroblasts from diabetic patients with or without nephropathy. *Nephrology Dialysis Transplantation*, 17(3):386–391, 2002.
- [69] Falguni Das, Nandini Ghosh-Choudhury, Nirmalya Dey, Amit Bera, Meenalakshmi M Mariappan, Balakuntalam S Kasinath, and Goutam Ghosh Choudhury. High glucose forces a positive feedback loop connecting akt kinase and foxo1 transcription factor to activate mtorc1 kinase for mesangial cell hypertrophy and matrix protein expression. *Journal of Biological Chemistry*, 289(47):32703–32716, 2014.
- [70] Richard C. Becker. COVID-19 update: Covid-19-associated coagulopathy. *Journal of Thrombosis and Thrombolysis*, May 2020.
- [71] Marco Viceconti, Gordon Clapworthy, Debora Testi, Fulvia Taddei, and Nigel McFarlane. Multimodal fusion of biomedical data at different temporal and dimensional scales. *Computer Methods and Programs in Biomedicine*, 102(3):227–237, June 2011.
- [72] W ELLIOTT. Circadian variation in blood pressure Implications for the elderly patient. *American Journal of Hypertension*, 12(2):43S–49S, February 1999.
- [73] Lewis A. Lipsitz. Loss of ‘complexity’ and aging. *JAMA*, 267(13):1806, April 1992.
- [74] Leon Glass, Michael C. Mackey, and Paul F. Zweifel. From clocks to chaos: The rhythms of life. *Physics Today*, 42(7):72–72, July 1989.
- [75] John P. Hirdes, Dinnus H. Frijters, and Gary F. Teare. The MDS-CHESS scale: A new measure to predict mortality in institutionalized older people. *Journal of the American Geriatrics Society*, 51(1):96–100, January 2003.
- [76] A E Ades, Nicky J Welton, Deborah Caldwell, Malcolm Price, Aicha Goubar, and Guobing Lu. Multiparameter evidence synthesis in epidemiology and medical decision-making. *Journal of Health Services Research & Policy*, 13(3\_suppl):12–22, October 2008.
- [77] Rudolf N. Cardinal. Clinical records anonymisation and text extraction (CRATE): an open-source software system. *BMC Medical Informatics and Decision Making*, 17(1), April 2017.
- [78] Tamara T. Müller and Pietro Lio. PECLIDES neuro: A personalisable clinical decision support system for neurological diseases. *Frontiers in Artificial Intelligence*, 3, April 2020.

- [79] Hiroshi Shionoiri, Shin-ichiro Ueda, Kohsuke Minamisawa, Mayumi Minamisawa, Izumi Takasaki, Koichi Sugimoto, Eiji Gotoh, and Masao Ishii. Pharmacokinetics and pharmacodynamics of benazepril in hypertensive patients with normal and impaired renal function. *Journal of cardiovascular pharmacology*, 20(3):348–357, 1992.
- [80] Shinji Hisatake, Shunsuke Kiuchi, Takayuki Kabuki, Takashi Oka, Shintaro Dobashi, and Takanori Ikeda. Serum angiotensin-converting enzyme 2 concentration and angiotensin-(1–7) concentration in patients with acute heart failure patients requiring emergency hospitalization. *Heart and vessels*, 32(3):303–308, 2017.
- [81] Gianna Toffolo, Richard N Bergman, Diane T Finegood, Charles R Bowden, and Claudio Cobelli. Quantitative estimation of beta cell sensitivity to glucose in the intact organism: a minimal model of insulin kinetics in the dog. *Diabetes*, 29(12):979–990, 1980.
- [82] Willy Malaisse, FRANCINE MALAISSE-LAGAE, and PETER H WRIGHT. A new method for the measurement in vitro of pancreatic insulin secretion. *Endocrinology*, 80(1):99–108, 1967.
- [83] Richard N Bergman, Lawrence S Phillips, and Claudio Cobelli. Physiologic evaluation of factors controlling glucose tolerance in man: measurement of insulin sensitivity and beta-cell glucose sensitivity from the response to intravenous glucose. *The Journal of clinical investigation*, 68(6):1456–1467, 1981.
- [84] Diane T Finegood. Application of the minimal model of glucose kinetics. *The Minimal Model Approach and Determinants of Glucose Tolerance*, 7:51–122, 1997.
- [85] Toshinori Imamura, Michael Koffler, J Harold Helderman, Dale Prince, Richard Thirlby, Lindsey Inman, and Roger H Unger. Severe diabetes induced in subtotally depancreatized dogs by sustained hyperglycemia. *Diabetes*, 37(5):600–609, 1988.

## A Appendix

### A.1 Website

#### Digital patients' dashboard

##### Description

Medicine is moving from reacting to a disease to prepare personalised and precision paths to well being. The complex and multi level pathophysiological patterns of most diseases require a systemic medicine approach and are challenging current medical therapies.

Here we present a Digital patient model that integrates, refine and extend recent specific mechanistic or phenomenological models of cardiovascular [1], RAS [2] and diabetic [3] processes. Our aim is twofold: analyse the modularity and composability of the models-building blocks of the Digital patient and to study the dynamical properties of well-being and disease states in a broader functional context. We present results from a number of experiments among which we characterise the dynamical impact of covid-19 and T2D diabetes on cardiovascular and inflammaging conditions. We tested these experiments under exercise and meals and drug regimen.

Common clinical parameters such as diastolic and systolic blood pressure, heart patterns, blood cell counts are usually evaluated as averages. Little importance is given to higher moments such as variances during the day or during a longer interval of time. The lack of continuous measures for most of the quantities has generated a medical practice that disregard of unobserved or partially observed data. Our composable model reveals interesting patterns, particularly fluctuations in blood pressure, particularly when the diabetic model is coupled with the RAS and the cardiovascular models under COVID acute infections.

##### References

- [1] Neal, M. L., & Bassingthwaite, J. B. (2007). Subject-specific model estimation of cardiac output and blood volume during hemorrhage. Cardiovascular engineering, 7(3), 97-120.
- [2] Pilvankar, M. R., Yong, H. L., & Ford Versypt, A. N. (2019). A Glucose-Dependent Pharmacokinetic/Pharmacodynamic Model of ACE Inhibition in Kidney Cells. Processes, 7(3), 131.
- [3] Topp, B., Promislow, K., Devries, G., Miura, R. M., & Finegood, D. T. (2000). A model of b-cell mass, insulin, and glucose kinetics: pathways to diabetes. Journal of theoretical biology, 206(4), 605.



##### Patient's characteristics

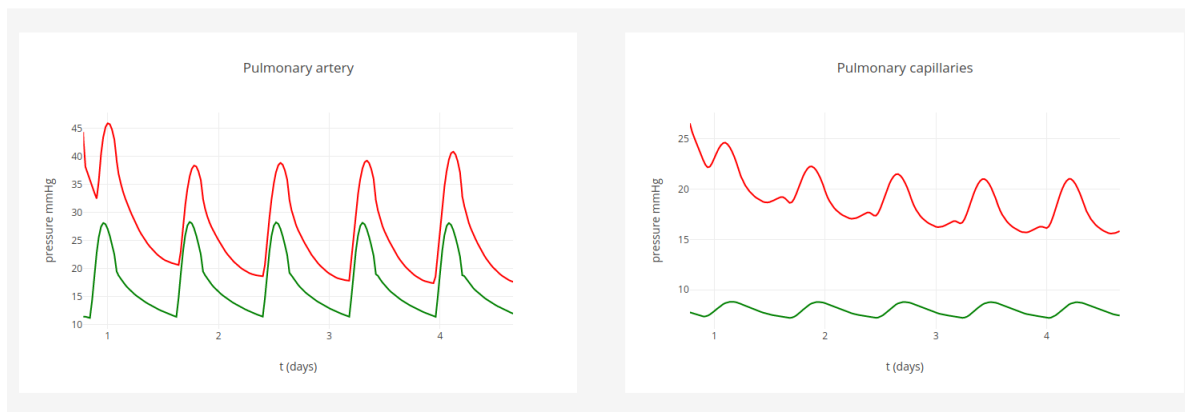
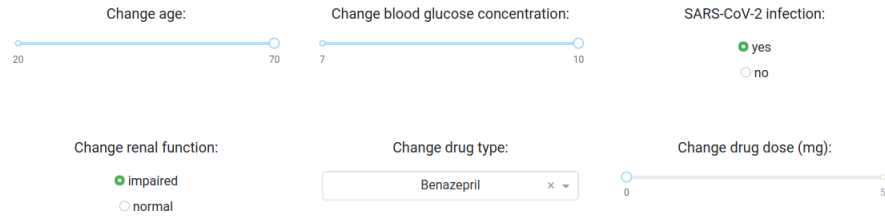


Figure 6: Website dashboard for Computational patients.

## A.2 Equations of the renin-angiotensin system

$$I = \frac{100[DRUG]^m}{[DRUG]_{50}^m + [DRUG]^m} \quad (15)$$

$$\frac{d[AGT]}{dt} = \overbrace{k_{AGT}}^{\text{production rate}} - \overbrace{(a_{Renin}G + b_{Renin})[AGT]}^{\text{renin-catalyzed conversion to ANG I}} - \overbrace{\frac{\ln(2)}{h_{AGT}}[AGT]}^{\text{degradation}} \quad (16)$$

$$\begin{aligned} \frac{d[Renin]}{dt} &= \overbrace{\frac{\ln 2}{h_{Renin}}[Renin]_0}^{\text{production rate}} \\ &+ \overbrace{\frac{k_{f,sys}[ANGII]_{0,sys}}{[ANGII]_0} \left( ([ANGII]_0 - [ANGII]) \left( 1 - ([ANGII]_0 - [ANGII]) \frac{[ANGII]_{0,sys}}{f_{sys}[ANGII]_0} \right) \right)}^{\text{ANG II inhibition feedback}} \\ &- \overbrace{\frac{\ln 2}{h_{Renin}}[Renin]}^{\text{degradation}} \end{aligned} \quad (17)$$

$$\begin{aligned} \frac{d[ANGI]}{dt} &= \overbrace{(a_{Renin}G + b_{Renin})[AGT]}^{\text{renin-catalyzed conversion of AGT}} + \overbrace{k_{Renin}([Renin] - [Renin]_0)}^{\text{ANG II feedback on renin}} \\ &- \overbrace{(a_{ACE}G + b_{ACE})[ANGI](1 - I)}^{\text{ACE-catalyzed conversion to ANG II subject to inhibition}} - \overbrace{(k_{NEP} + k_{ACE2})[ANGI]}^{\text{conversion to ANG-(1-7) and ANG-(1-9)}} \\ &- \overbrace{\frac{\ln 2}{h_{ANGI}}[ANGI]}^{\text{degradation}} \end{aligned} \quad (18)$$

$$\begin{aligned} \frac{d[ANGII]}{dt} &= \overbrace{(a_{ACE}G + b_{ACE})[ANGI](1 - I)}^{\text{ACE-catalyzed conversion to ANG II subject to inhibition}} \\ &- \overbrace{(k_{ACE2} + (a_{AT1}G + b_{AT1}) + k_{AT2} + k_{APA})[ANGII]}^{\text{conversion to AT1R, AT2R, APA, and ANG-(1-7)}} \\ &- \overbrace{\frac{\ln 2}{h_{ANGII}}[ANGII]}^{\text{degradation}} \end{aligned} \quad (19)$$

## A.3 Equations of the open-loop circulatory model

### A.3.1 Four-chambered heart

$$t \geq t_{HB}(n+1) - PR_{int} - offv \implies \begin{cases} HR_a = \frac{1}{HP/60} \\ T_{s_a} = Ts1_a \sqrt{\frac{Ts2}{HR_a/60}} \\ t_{Pwave} = t_{HB} - PR_{int} - offv \\ n = n + 1 \end{cases} \quad (20)$$



$$t \geq t_{HB(m+1)-offv} \implies \begin{cases} HR_v = \frac{1}{HP/60} \\ T_{s_v} = Ts1_v \sqrt{\frac{Ts2}{HR_v/60}} \\ t_{Rwave} = t_{HB} - offv \\ m = n \\ V_{var,i,vs0} = \begin{cases} V_{i,vd0} & V_{i,v} < V_{i,vd0} \\ V_{i,vs0} & V_{i,v} > EDV_{i_v} \\ V_{i,vs0} - V_{i,vd0} \frac{V_{i,v} - V_{i,vd0}}{EDV_{i,v} - V_{i,vd0}} + V_{i,vd0} & V_{i,vd0} \leq V_{i,v} \leq EDV_{i_v} \end{cases} \\ af_{con2} = af_{con} \end{cases} \quad (21)$$

$$HR = HR_v \quad (22)$$

$$E_{max,i,v} = K_{e,i,v} E_{max,i,v1} \quad (23)$$

$$t_{a,REL} = t - t_{Pwave} \quad (24)$$

$$t_{v,REL} = t - t_{Rwave} \quad (25)$$

$$y_i = \begin{cases} \frac{1 - \cos \pi \frac{t_{i,REL}}{T_{s,i}}}{2} & 0 \leq t_{i,REL} < T_{s,i} \\ \frac{1 + \cos 2\pi \frac{t_{i,REL} - T_{s,i}}{T_{s,i}}}{2} & T_{s,i} \leq t_{i,REL} < 1.5T_{s,i} \\ 0 & t_{i,REL} \geq 1.5T_{s,i} \end{cases} \quad (26)$$

$$E_{i,j} = y_j(E_{max,i,j} - E_{min,i,j}) + E_{min,i,j} \quad (27)$$

$$V_{i,a,0} = (1 - y_a)(V_{i,a,d0} - V_{i,a,s0}) + V_{i,a,s0} \quad (28)$$

$$V_{i,v,0} = (1 - y_v)(V_{i,v,d0} - V_{var,i,vs0}) + V_{var,i,vs0} \quad (29)$$

$$\psi(v) = K_{xp} \frac{1}{e^{v/K_{xv}} - 1} \quad (30)$$

$$P_{i,a} = E_{i,a}(V_{i,a} - V_{i,a0}) - \psi(V_{i,a}) \quad (31)$$

$$P_{i,v} = E_{i,v}(V_{i,v} - V_{i,v0})af_{con2} - \psi(V_{i,v}) \quad (32)$$

$$F_{i,a} = \begin{cases} \frac{P_{i,a} - P_{i,v}}{R_{i,a}} & P_{i,a} > P_{i,v} \\ 0 & P_{i,a} \leq P_{i,v} \end{cases} \quad (33)$$

$$F_{r,v} = \begin{cases} \frac{P_{r,v} - P_{pap}}{R_{r,v}} & P_{r,v} > P_{pap} \\ 0 & P_{r,v} \leq P_{pap} \end{cases} \quad (34)$$

$$F_{l,v} = \begin{cases} \frac{P_{l,v} - P_{aop}}{R_{l,v}} & P_{l,v} > P_{aop} \\ 0 & P_{l,v} \leq P_{aop} \end{cases} \quad (35)$$

$$\frac{dV_{r,a}}{dt} = \quad (36)$$

$$\frac{dV_{r,a}}{dt} = \frac{F_{vc} + F_{corvn}}{F_{r,a}} \quad (37)$$

$$\frac{dV_{r,v}}{dt} = \frac{F_{r,a}}{F_{rv}} \quad (38)$$

$$\frac{dV_{l,a}}{dt} = \frac{F_{pv}}{F_{l,a}} \quad (39)$$

$$\frac{dV_{l,v}}{dt} = \frac{F_{l,a}}{F_{l,v}} \quad (40)$$

### A.3.2 Systemic circulation

$$P_{vc} = \begin{cases} K_1(V_{vc} - V_{vc0}) - \psi(V_{vc}) & V_{vc} > V_{vc0} \\ D_2 + K_2 e^{V_{vc}/V_{min,vc}} - \psi(V_{vc}) & V_{vc} \leq V_{vc0} \end{cases} \quad (41)$$

$$CO_{mod} = F_{rv,sm} \quad (42)$$

$$SV = \frac{CO_{mod}}{HR} \quad (43)$$

$$ABP_{shift} = ABP_{meas}(t - offv) \quad (44)$$

$$K_v = K_{v1} K_{sv} \quad (45)$$

$$MAP_{mod} = \frac{R_{crb} \left[ R_{taod} AOF_{mod} - R_{taod} F_{aod} + \frac{V_{aod} - V_{aod0}}{C_{aod}} - \psi(V_{aod}) \right] + P_{vc} R_{taod}}{R_{crb} + R_{taod}} \quad (46)$$

$$P_{aod} = ABP_{shift} \quad (47)$$

$$P_{sap} = \frac{V_{sap} - V_{sap0}}{C_{sap}} - \psi(V_{sap}) \quad (48)$$

$$P_{sa,a} = K_c \log_{10} \left[ \frac{V_{sa} - V_{sa0}}{D_o} + 1 \right] \quad (49)$$

$$P_{sa,p} = K_{p1} e^{\tau_p(V_{sa} - V_{sa0})} + K_{p2} (V_{sa} - V_{sa0})^2 \quad (50)$$

$$P_{sa} = f_{vaso}P_{sa,a} + (1 - f_{vaso})P_{sa,p} \quad (51)$$

$$P_{sc} = \frac{V_{sc} - V_{sc0}}{C_{sc}} - \psi(V_{sc}) \quad (52)$$

$$P_{sv} = -K_v \log_{10} \left[ \frac{V_{max,sv}}{V_{sv}} - 0.99 \right] \quad (53)$$

$$R_{sa} = K_r \left( e^{4f_{vaso}} + \frac{V_{sa,max}^2}{V_{sa}^2} \right) + R_{sa0} \quad (54)$$

$$R_{vc} = K_R \frac{V_{max,vc}^2}{V_{vc}^2} + R_0 \quad (55)$$

$$F_{crb} = \frac{MAP_{mod} - P_{vc}}{R_{crb}} \quad (56)$$

$$F_{sap} = \frac{P_{sap} - P_{sa}}{R_{sap}} \quad (57)$$

$$F_{sa} = \frac{P_{sa} - P_{sc}}{R_{sa}} \quad (58)$$

$$F_{sc} = \frac{P_{sc} - P_{sv}}{R_{sc}} \quad (59)$$

$$F_{sv} = \frac{P_{sv} - P_{vc}}{R_{sv}} \quad (60)$$

$$F_{vc} = \frac{P_{vc} - P_{ra}}{R_{vc}} \quad (61)$$

$$\frac{dV_{aop}}{dt} = \frac{P_{aop} - \frac{V_{aop} - V_{aop0}}{C_{aop}}}{R_{taop}} \quad (62)$$

$$\frac{dV_{aod}}{dt} = AOF_{mod} - F_{aod} - F_{crb} \quad (63)$$

$$\frac{dV_{sa}}{dt} = F_{sap} - F_{sa} \quad (64)$$

$$\frac{dV_{sap}}{dt} = F_{aod} - F_{sap} \quad (65)$$

$$\frac{dV_{sc}}{dt} = F_{sa} - F_{sc} \quad (66)$$

$$\frac{dV_{sv}}{dt} = F_{sc} - F_{sv} \quad (67)$$

$$\frac{dV_{vc}}{dt} = F_{sv} + F_{crb} - F_{vc} \quad (68)$$

$$\frac{dAOF_{mod}}{dt} = (MAP_{meas} - MAP_{mod}) \frac{K_{comap}}{60} \quad (69)$$

$$\frac{dF_{rv,sm}}{dt} = \frac{F_{rv} - F_{rv,sm}}{\tau_{co}} \quad (70)$$

$$\frac{dF_{aod}}{dt} = \frac{MAP_{mod} - F_{aod}R_{aod} - P_{sap}}{L_{aod}} \quad (71)$$

$$\frac{dP_{paop}}{dt} = \frac{F_{lv} - \frac{dV_{aop}}{dt} - F_{aop} - F_{corepi}}{C_{corepi}} \quad (72)$$

$$\frac{dMAP_{meas}}{dt} = \frac{ABP_{shift} - MAP_{meas}}{\tau_{MAP}} \quad (73)$$

$$\frac{dCO_{mea}}{dt} = \frac{PAF_{meas} - CO_{mea}}{\tau_{co}} \quad (74)$$

$$\frac{dABP_{fol}}{dt} = \frac{ABP_{shift} - ABP_{fol}}{\tau_{ABP}} \quad (75)$$

### A.3.3 Pulmonary circulation

$$P_{pap} = \begin{cases} P_{pap1} = \frac{R_{tpap}P_{rv} - R_{rv}F_{pap}R_{tpap} + \left(R_{rv}\frac{V_{pap} - V_{pap0}}{C_{pap}} - \psi(V_{pap})\right)}{R_{tpap} + R_{rv}} & P_{rv} > P_{pap1} \\ P_{pap2} = \frac{-R_{rv}F_{pap}R_{tpap} + \left(R_{rv}\frac{V_{pap} - V_{pap0}}{C_{pap}} - \psi(V_{pap})\right)}{R_{rv}} & P_{rv} \leq P_{pap1} \end{cases} \quad (76)$$

$$P_{pad} = F_{pap}R_{tpad} - F_{pad}R_{tpad} + \frac{V_{pad} - V_{pad0}}{C_{pad}} - \psi(V_{pad}) \quad (77)$$

$$V_{p,i} = \frac{V_{p,i} - V_{p,i,0}}{C_{p,i}} - \psi(V_{p,i}) \quad (78)$$

$$F_{ps} = \frac{P_{pa} - P_{pv}}{R_{ps}} \quad (79)$$

$$F_{pa} = \frac{P_{pa} - P_{pc}}{R_{pa}} \quad (80)$$

$$F_{pc} = \frac{P_{pc} - P_{pv}}{R_{pc}} \quad (81)$$

$$F_{pv} = \frac{P_{pv} - P_{pa}}{R_{pv}} \quad (82)$$

$$\frac{dF_{pap}}{dt} = \frac{P_{pap} - P_{pad} - F_{pap}R_{pap}}{L_{pap}} \quad (83)$$

$$\frac{dF_{pad}}{dt} = \frac{P_{pad} - P_{pa} - F_{pad}R_{pad}}{L_{pad}} \quad (84)$$

$$\frac{dV_{pad}}{dt} = F_{pap} - F_{pad} \quad (85)$$

$$\frac{dV_{pap}}{dt} = F_{rv} - F_{pap} \quad (86)$$

$$\frac{dV_{pa}}{dt} = F_{pad} - F_{ps} - F_{pa} \quad (87)$$

$$\frac{dV_{pc}}{dt} = F_{pa} - F_{pc} \quad (88)$$

$$\frac{dV_{pv}}{dt} = F_{pc} + F_{ps} - F_{pv} \quad (89)$$

#### A.3.4 Coronary circulation

$$P_{corepi} = P_{aop} \quad (90)$$

$$P_{corintra} = \frac{V_{corintra} - V_{corintra0}}{C_{corintra}} - \psi(V) \quad (91)$$

$$P_{corcap} = \frac{V_{corcap} - V_{corcap0}}{C_{corcap}} - \psi(V_{corcap}) \quad (92)$$

$$P_{corvn} = \frac{V_{corvn} - V_{corvn0}}{C_{corvn}} - \psi(V_{corvn}) \quad (93)$$

$$P_{im} = \left\lfloor \frac{P_{lv}}{2} \right\rfloor \quad (94)$$

$$P_{corintrac} = P_{corintra} + P_{im} \quad (95)$$

$$P_{corcapc} = P_{corcap} + P_{im} \quad (96)$$

$$P_{corvnc} = P_{corvn} \quad (97)$$

$$F_{corepi} = \frac{P_{corepi} - P_{corintrac}}{R_{corepi}} \quad (98)$$

$$F_{corintra} = \frac{P_{corintrac} - P_{corcapc}}{R_{corintra}} \quad (99)$$

$$F_{corcap} = \frac{P_{corcapc} - P_{corvnc}}{R_{corcap}} \quad (100)$$

$$F_{corvn} = \frac{P_{corvnc} - P_{ra}}{R_{corvn}} \quad (101)$$

$$\frac{dV_{corepi}}{dt} = F_{lv} - \frac{dV_{vaop}}{dt} - F_{aop} - F_{corepi} \quad (102)$$

$$\frac{dV_{corintra}}{dt} = F_{corepi} - F_{corintra} \quad (103)$$

$$\frac{dV_{corcap}}{dt} = F_{corintra} - F_{corcap} \quad (104)$$

$$\frac{dV_{corvn}}{dt} = F_{corcap} - F_{corvn} \quad (105)$$

### A.3.5 Baroreceptor

$$b_{vaso} = 1 - a_{vaso} \quad (106)$$

$$f_{vaso} = a_{vaso} + \frac{b_{vaso}}{e^{\tau_{vaso}(N_{vaso} - N_{o,vaso})}} + 1 \quad (107)$$

$$N_{br,t} = \frac{dN_{br}}{dt} \quad (108)$$

$$\frac{dN_{br,t}}{dt} = \frac{-(a_2 + a)N_{br,t} - N_{br} + K \left( ABP_{shift} + a_1 \frac{dABP_{fol}}{dt} \right)}{a_2 a} \quad (109)$$

$$\frac{dN_i}{dt} = \begin{cases} \frac{-N_i + K_i N_{br}(t - l_i)}{T_i} & t - t_{HB}(0) > l_i \\ 0 & t - t_{HB}(0) \leq l_i \end{cases} \quad (110)$$

### A.3.6 Blood volumes

$$V_{corcic} = V_{corepi} + V_{corintra} + V_{corcap} + V_{corvn} \quad (111)$$

$$V_{heart} = V_{ra} + V_{rv} + V_{la} + V_{lv} + V_{corcic} \quad (112)$$

$$V_{sysart} = V_{aop} + V_{aod} + V_{sap} + V_{sa} \quad (113)$$

$$V_{sysven} = V_{sv} + V_{vc} \quad (114)$$

$$V_{pulart} = V_{pap} + V_{pad} + V_{pa} \quad (115)$$

$$TBV = V_{heart} + V_{sysart} + V_{sc} + V_{sysven} + V_{pulart} + V_{pc} + V_{pv} \quad (116)$$



#### A.4 Parameters of the renin-angiotensin system

Table 3: Pharmacokinetic parameters

Parameter	NRF	IRF	Units	Sources	Description
$k_a$	1.907	1.645	$h^{-1}$	[46, 79]	absorption rate constant
$k_e$	$1.33 \times 10^{-1}$	$3.45 \times 10^{-2}$	$h^{-1}$	[46, 79]	elimination rate constant
$V/F$	$7.09 \times 10^4$	$1.07 \times 10^5$	$mL$	[46, 79]	ratio of the volume of distribution to the fraction of the drug absorbed

Table 4: Pharmacodynamic parameters

Parameter	Value	Units	Sources	Description
$k_{AGT}$	$2.27 \times 10^6$	$nmol/L/h$	[48, 14]	constant production rate of AGT
$k_{Renin}$	$6.44 \times 10^4$	$h^{-1}$	[46, 14]	ANG-I production rate due to renin
$k_{NEP}$	0.583	$h^{-1}$	[48, 14]	NEP-catalyzed conversion rate from ANG-I to ANG-(1-7)
$k_{AT2}$	25.1	$h^{-1}$	[48, 14]	rate parameter for binding of ANG II to AT1R
$k_{APA}$	43.6	$h^{-1}$	[48, 14]	APA-catalyzed conversion rate from ANG-II to ANG-III
$h_{AGT}$	10.0	$h$	[49, 48, 14]	AGT half-life degradation rate
$h_{Renin}$	0.250	$h$	[48, 14]	renin half-life degradation rate
$h_{ANGI}$	$1.72 \times 10^{-4}$	$h$	[49, 48, 14]	ANG-I half-life degradation rate
$h_{ANGII}$	$5 \times 10^{-3}$	$h$	[49, 48, 14]	ANG-II half-life degradation rate
$[Drug]_{50}$	2.20	$ng/mL$	[79, 48, 14]	drug concentration yielding 50% inhibition
$m$	0.99	-	[79, 48, 14]	degree of sigmoidicity of the Hill function
$a_{Renin}$	$5.47 \times 10^{-4}$	$L/mmol/h$	[48, 14]	slope of the linear dependence of renin from glucose
$b_{Renin}$	$6.16 \times 10^{-11}$	$h^{-1}$	[48, 14]	intercept of the linear dependence of renin from glucose
$a_{ACE}$	0.889	$L/mmol/h$	[48, 14]	slope of the linear dependence of ACE from glucose
$b_{ACE}$	163	$h^{-1}$	[48, 14]	intercept of the linear dependence of ACE from glucose
$a_{AT1}$	2.55	$L/mmol/h$	[48, 14]	slope of the linear dependence of AT1R from glucose
$b_{AT1}$	464	$h^{-1}$	[48, 14]	intercept of the linear dependence of AT1R from glucose
$k_{f,sys}$	$6.25 \times 10^{-2}$	$h^{-1}$	[46, 14]	ANG-II feedback parameter on renin

Table 4 continued from previous page

Parameter	Value	Units	Sources	Description
$f_{sys}$	0.397	$nmol/L$	[46, 14]	ANG-II feedback parameter on renin
$[AGT]_0$	$1.70 \times 10^7$	$nmol/L$	[48, 14]	AGT initial concentration
$[Renin]_0$	$2.06 \times 10^{-4}$	$nmol/L$	[46, 14]	renin initial concentration
$[ANGI]_0$	271	$nmol/L$	[48, 14]	ANG-I initial concentration
$[ANGII]_0$	21.0	$nmol/L$	[48, 14]	ANG-II initial concentration
$[ANGII]_{0,sysNRF}$	$1.65 \times 10^{-2}$	$nmol/L$	[46, 14]	systemic ANG-II initial concentration for normal renal individuals
$[ANGII]_{0,sysIRF}$	$2.05 \times 10^{-2}$	$nmol/L$	[46, 14]	systemic ANG-II initial concentration for impaired renal individuals
$h_{ANG17}$	0.5	$h$	[49]	ANG-17 half-life degradation rate
$[ANG17]_0$	9.858	$nmol/L$	[80]	ANG-17 initial concentration
$h_{AT1R}$	0.2	$h$	[49]	AT1R half-life degradation rate
$[AT1R]_0$	16.2	$nmol/L$	[80]	AT1R initial concentration
$h_{AT2R}$	0.2	$h$	[49]	AT2R half-life degradation rate
$[AT2R]_0$	5.4	$nmol/L$	[80]	AT2R initial concentration
$k_{ACE2,0}$	0.385	$h^{-1}$	[48, 14]	ACE-catalyzed conversion rate from ANG-II to ANG-(1-7)
$s_I$	0.1	$h^{-1}L/nmol$	-	severity of SARS-CoV-2 infection
$e_{AI}$	0.347	-	-	efficiency of anti-inflammatory pathways

## A.5 Parameters of the diabetic model

Table 5: Diabetic parameters

Parameter	Value	Units	Sources	Description
$k$	432	$d^{-1}$	[81]	combined insulin uptake at the liver, kidneys, and insulin receptors
$\alpha$	20000	$mg^2dl^{-2}$	[82]	glucose concentration yielding 50% of insulin secretion
$\sigma$	43.2	$\mu U \text{ } ml^{-1}d^{-1}$	[83, 82, 81]	maximal rate secretion of insulin by $\beta$ cells
$R_0$	864	$mg \text{ } dl^{-1}d^{-1}$	[83, 84]	net rate of production at zero glucose
$R_1$	1	$ml \text{ } dl^{-1}g^{-1}$	-	net rate of glucose increase due to meals

Table 5 continued from previous page

Parameter	Value	Units	Sources	Description
$R_2$	0.1	$ml\ dl^{-1}\ kcal^{-1}$	-	net rate of glucose consumption due to workouts
$EG_0$	0.44	$d^{-1}$	[83, 84]	total glucose effectiveness at zero insulin
$SI$ (normal)	1.62	$ml\ \mu U^{-1} d^{-1}$	[84]	normal insulin sensitivity
$SI$ (diabetic)	0.52	$ml\ \mu U^{-1} d^{-1}$	[84]	diabetic insulin sensitivity
$r_0$	0.06	$d^{-1}$	[83, 85, 84]	death rate at zero glucose
$r_1$	0.00084	$mg^{-1} dl\ d^{-1}$	[83, 85, 84]	I-order coefficient for $\beta$ cell replication
$r_2$	0.0000024	$mg^{-2} dl\ d^{-1}$	[83, 85, 84]	II-order coefficient for $\beta$ cell replication
$i_0$	87	-	[13]	insulin resistance self-inhibition rate
$m$	2	-	[13]	insulin resistance progression rate due to pro-inflammatory cytokines
$q$	0.017	$ml/\mu U$	[13]	insulin resistance progression rate due to insulin concentration
$I_0$	13.59	$\mu U/ml$	[13]	initial insulin concentration
$G_0$	100	$ml/dl$	[13]	initial glucose concentration
$\beta_{f,0}$	407.73	-	[13]	number of functional $\beta$ -cells
$I_{R,0}$	0.359	-	-	initial insulin resistance

## A.6 Parameters of the stiffness model

Table 6: Stiffness parameters

Parameter	Value	Units	Sources	Description
$k_{SARS}$	0.15	$h$		inflammation rate due to SARS-CoV-2
$k_D$	0.001	$mL/ng$		inflammation rate due to ACEi surplus
$k_G$	0.1	$L/mmol$		inflammation rate due to glucose surplus
$k_{eff}$ (healthy state)	0.035	-		anti-inflammatory response rate
$k_{eff}$ (during infection)	0.693	-		anti-inflammatory response rate
$\beta_1$	0.006	-		compliance reduction rate due to ageing
$\beta_0$	1.2	-		compliance reduction intercept due to ageing

Table 6 continued from previous page

Parameter	Value	Units	Description
$IR_0$	0.385	-	inflammatory response initial condition

### A.7 Parameters of the open-loop circulatory model

Parameter	Value	Units	Description
$Ts1v$	0.349	<i>sec</i>	Scaler to set ventricular systolic fraction of heart cycle
$Ts1a$	0.2	<i>sec</i>	Scaler to set atrial systolic fraction of heart cycle
$Ts2$	1	<i>hz</i>	Unit balance scalar for $Tsa$ and $Tsv$ functions
$offv$	0.0263	<i>sec</i>	Parameter to match model and measured end-diastolic ABP
$Vlvd0$	71.816	<i>ml</i>	Unstressed end-diastolic left ventricle volume
$Vlvs0$	23.699	<i>ml</i>	Unstressed end-systolic left ventricle volume
$Vrvd0$	102.881	<i>ml</i>	Unstressed end-diastolic right ventricle volume
$Vrvs0$	53.498	<i>ml</i>	Unstressed end-systolic right ventricle volume
$Vlad0$	70	<i>ml</i>	Unstressed end-diastolic left atrium volume
$Vlas0$	40	<i>ml</i>	Unstressed end-systolic left atrium volume
$Vrad0$	60	<i>ml</i>	Unstressed end-diastolic right atrium volume
$Vras0$	53	<i>ml</i>	Unstressed end-systolic right atrium volume
$Rra$	0.001	$mmHg\ s\ ml^{-1}$	Tricuspid valve resistance
$Rla$	0.001	$mmHg\ s\ ml^{-2}$	Mitral valve resistance
$Rlv$	0.0001	$mmHg\ s\ ml^{-3}$	Aortic valve resistance
$Rrv$	0.0001	$mmHg\ s\ ml^{-4}$	Pulmonary valve resistance
$PRint$	0.12	<i>sec</i>	Difference in atrial, ventricular activation times
$KElv$	1		Scaling factor for maximum left ventricular elastance
$KErv$	1		Scaling factor for maximum right ventricular elastance
$E_{maxlv1}$	5.4	$mmHg/ml$	Maximum elastance of first left ventricle component

Table 7 continued from previous page

Parameter	Value	Units	Description
$E_{minlv}$	0.09	$mmHg/ml$	Minimum elastance of first left ventricle component
$E_{maxrv1}$	0.53	$mmHg/ml$	Maximum elastance of first right ventricle component
$E_{minrv}$	0.0343	$mmHg/ml$	Minimum elastance of first right ventricle component
$EDVLV$	125.993	$ml$	
$EDVRV$	175.865	$ml$	
$E_{maxra}$	0.13	$mmHg/ml$	Maximum elastance right ventricle
$E_{minra}$	0.085	$mmHg/ml$	Minimum elastance left ventricle
$E_{maxla}$	0.299	$mmHg/ml$	Maximum elastance right ventricle
$E_{minla}$	0.185	$mmHg/ml$	Minimum elastance left ventricle
$KCOMAP$	3	$L/mmHg/min^2$	
$Raop$	0.0001	$mmHg \sec ml^{-1}$	Proximal aortic resistance
$Rtaop$	0.02	$mmHg \sec ml^{-1}$	Transmural proximal aortic resistance
$Rcrb$	6.8284	$mmHg \sec ml^{-1}$	Cerebral circulation resistance
$Raod$	0.0129	$mmHg \sec ml^{-1}$	Distal aortic resistance
$Rtaod$	1	$mmHg \sec ml^{-1}$	Transmural distal aortic resistance
$Rsap$	0.003	$mmHg \sec ml^{-1}$	Systemic arteriolar resistance
$Rsc$	0.155	$mmHg \sec ml^{-1}$	Systemic capillaries resistance
$Rsv$	0.138	$mmHg \sec ml^{-1}$	Systemic veins resistance
$Caop$	0.263	$ml \ mmHg^{-1}$	Aortic proximal compliance
$Caod$	0.639	$ml \ mmHg^{-1}$	Aortic distal compliance
$Csap$	1.482	$ml \ mmHg^{-1}$	Systemic arterioles compliance
$Csc$	5.767	$ml \ mmHg^{-1}$	Systemic capillaries compliance
$Vaop0$	9.520	$ml$	Proximal aorta unstressed volume
$Vaod0$	23.11	$ml$	Distal aorta unstressed volume
$Vsap0$	52.94	$ml$	Systemic arteries unstressed volume
$Vsc0$	71.02	$ml$	Systemic capillaries unstressed volume

Table 7 continued from previous page

Parameter	Value	Units	Description
$Laop$	$1e - 05$	$mmHg \text{ sec}^2 \text{ ml}^{-1}$	Proximal aorta inertance
$Laod$	$2e - 05$	$mmHg \text{ sec}^2 \text{ ml}^{-1}$	Distal aorta inertance
$Kc$	497.785	$mmHg$	Active vasomotor tone scaling parameter for systemic arterial pressure
$Do$	50	$ml$	Active vasomotor tone volume parameter for systemic arterial pressure
$Vsa0$	485.762	$ml$	Minimal volume of systemic arteries
$Vsa_{max}$	577.711	$ml$	Maximal luminal volume of systemic arteries
$Kp1$	0.0299	$mmHg$	Passive vasomotor tone scaling parameter for systemic arterial pressure
$Kp2$	0.05	$mmHg \text{ ml}^{-2}$	Passive vasomotor tone scaling parameter for systemic arterial pressure
$Kr$	0.01	$mmHg \text{ sec ml}^{-1}$	Pressure scaling constant for systemic arterial resistance
$Rsa0$	0.581	$mmHg \text{ sec/ml}$	Offset parameter for systemic arteriolar resistance
$\tau_p$	0.1	$ml^{-1}$	Passive vasomotor tone constant for systemic arterial pressure
$Ksv$	0.74		Scaling factor used to optimize systemic venous pressure-volume relationship
$Kv1$	30.21	$mmHg$	Scaling factor for systemic venous pressure
$Vmax_{sv}$	3379.55	$ml$	Maximal volume of lumped systemic veins
$D2$	-5	$mmHg$	Offsetting constant for partially collapsed Vena cava pressure
$K1$	0.046	$mmHg \text{ ml}^{-1}$	Scaling factor for Vena cava PV relationship
$K2$	0.374	$mmHg$	Scaling factor for partially collapsed Vena cava pressure
$KR$	0.001	$mmHg \text{ sec ml}^{-1}$	Scaling factor for Vena cava resistance
$R0$	0.025	$mmHg \text{ sec ml}^{-1}$	Vena cava resistance offset parameter
$Vvc0$	129.649	$ml$	Unstressed volume of Vena cava
$Vmax_{vc}$	350.53	$ml$	Maximum volume of Vena cava
$Vmin_{vc}$	50.01	$ml$	Minimum volume of Vena cava
$\tau_{CO}$	15	$sec$	Cardiac output equation time constant
$Kxp$	2	$mmHg$	P-V curve shaping parameter
$Kxv$	8	$ml$	P-V curve shaping parameter
$Kxv1$	1	$ml$	P-V curve shaping parameter

Table 7 continued from previous page

Parameter	Value	Units	Description
$Kxp1$	1	$mmHg$	P-V curve shaping parameter
$\tau_{MAP}$	2	$sec$	Time constant for mean arterial pressure ODE
$\tau_{ABP}$	0.001	$sec$	Time constant for ABP follower
$Rtpap$	0.1	$mmHg \ sec \ ml^{-1}$	Proximal pulmonary arterial transmural resistance
$Rtpad$	0.2	$mmHg \ sec \ ml^{-1}$	Distal pulmonary arterial transmural resistance
$Rpap$	0.0001	$mmHg \ sec \ ml^{-1}$	Proximal pulmonary resistance
$Rpad$	0.0299	$mmHg \ sec \ ml^{-1}$	Distal proximal pulmonary resistance
$Rps$	4.333	$mmHg \ sec \ ml^{-1}$	Pulmonary shunt resistance
$Rpa$	0.057	$mmHg \ sec \ ml^{-1}$	Pulmonary arterioles resistance
$Rpc$	0.032	$mmHg \ sec \ ml^{-1}$	Pulmonary capillaries resistance
$Rpv$	0.0001	$mmHg \ sec \ ml^{-1}$	Pulmonary veins resistance
$Cpap$	1.445	$ml \ mmHg^{-1}$	Proximal pulmonary arterial compliance
$Cpad$	2.531	$ml \ mmHg^{-1}$	Distal pulmonary arterial compliance
$Cpa$	3.102	$ml \ mmHg^{-1}$	Pulmonary arterioles compliance
$Cpc$	9.117	$ml \ mmHg^{-1}$	Pulmonary capillaries compliance
$Cpv$	52.267	$ml \ mmHg^{-1}$	Pulmonary veins compliance
$Vpap0$	9.81	$ml$	Proximal pulmonary artery unstressed volume
$Vpad0$	17.16	$ml$	Distal pulmonary artery unstressed volume
$Vpa0$	17.16	$ml$	Small pulmonary arteries unstressed volume
$Vpc0$	29.42	$ml$	Pulmonary capillaries unstressed volume
$Vpv0$	29.597	$ml$	Pulmonary veins unstressed volume
$Lpap$	0.00018	$mmHg \ sec^2 \ ml^{-1}$	Proximal arterial inertance
$Lpad$	0.00019	$mmHg \ sec^2 \ ml^{-1}$	Distal pulmonary artery inertance
$Rcorepi$	5.285	$s \ ml^{-1} \ mmHg$	Proximal epicardial arteries resistance
$Rcorintra$	10.147	$s \ ml^{-1} \ mmHg$	Distal epicardial arteries resistance
$Rcorcap$	4.228	$s \ ml^{-1} \ mmHg$	Coronary capillaries resistance

Table 7 continued from previous page

Parameter	Value	Units	Description
$R_{corvn}$	1.48	$s\ ml^{-1}\ mmHg$	Small coronary veins resistance
$C_{corepi}$	0.074	$ml/mmHg$	Compliance of proximal epicardial arteries
$C_{corintra}$	0.134	$ml/mmHg$	Compliance of distal epicardial arteries
$C_{corcap}$	0.94	$ml/mmHg$	Compliance of coronary capillaries
$C_{corvn}$	2.45	$ml/mmHg$	Compliance of small coronary veins
$V_{corepi0}$	2.69	$ml$	Epicardial arteries unstressed volume
$V_{corintra0}$	2.685	$ml$	Intramyocardial arteries unstressed volume
$V_{corcap0}$	2.523	$ml$	Coronary capillaries unstressed volume
$V_{corvn0}$	2.493	$ml$	Coronary veins unstressed volume
$a$	0.001	$sec$	Time constant for baroreceptor firing rate
$a1$	0.036	$sec$	Time constant for baroreceptor firing rate
$a2$	0.0018	$sec$	Time constant for baroreceptor firing rate
$K$	0.991	$sec^{-1}\ mmHg^{-1}$	Baroreceptor gain (used to account for units)
$K_{con}$	1		CNS gain for contractility control
$T_{con}$	10	$sec$	CNS time parameter for contractility control
$l_{con}$	3	$sec$	CNS time delay for contractility control
$a_{con}$	0.299		Time constant for efferent contractility firing
$b_{con}$	0.699		Time constant for efferent sympathetic contractility firing
$\tau_{con}$	0.04	$sec$	Time parameter for efferent sympathetic contractility firing
$No_{con}$	110	$sec^{-1}$	Frequency parameter for efferent sympathetic contractility firing
$K_{vaso}$	1		CNS gain for vasomotor tone control
$T_{vaso}$	6	$sec$	CNS time parameter for vasomotor tone control
$l_{vaso}$	3	$sec$	CNS time delay for vasomotor tone control
$a_{vaso}$	-0.466		Time constant for efferent vasomotor tone firing
$\tau_{vaso}$	0.04	$sec$	Time parameter for efferent vasomotor tone firing
$No_{vaso}$	110	$sec^{-1}$	Frequency parameter for efferent vasomotor tone firing



Table 7 continued from previous page

Parameter	Value	Units	Description
$a_{min}$	-2.806		Contractility control offset
$b_{min}$	0.699		Contractility control offset
$Ka$	5		Contractility control scaling factor
$Kb$	0.5		Contractility control scaling factor